iScience

CellPress

Article

Targeted Drug-Loaded Chemical Probe Staining Assay to Predict Therapy Response and Function as an Independent Pathological Marker

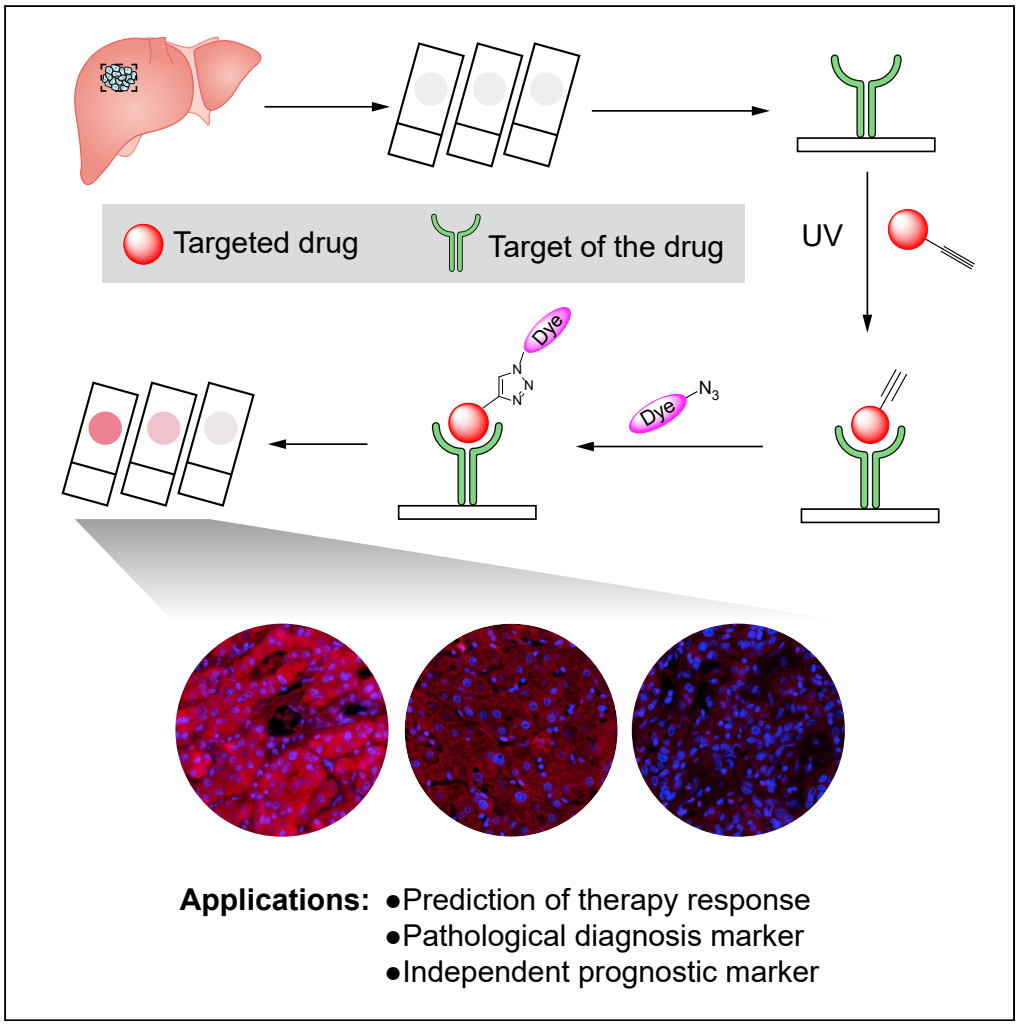

Heng Zhang, Wei-long Zhong, Bo Sun, ..., Shuang Chen, Cheng Yang, Tao Sun

honggang.zhou@nankai.edu.cn (H.-g.Z.)
shuang7332@163.com (S.C.)
cheng.yang@nankai.edu.cn (C.Y.)
tao.sun@nankai.edu.cn (T.S.)

HIGHLIGHTS

The assay could be used for the rapid sensitivity detection of multi-target drugs

The assay could serve as an auxiliary technology for NGS and PDX

Sorafenib had multiple unknown primary contribution targets

Drug-probe staining could be used as an independent diagnostic and prognostic marker

DATA AND CODE AVAILABILITY

GSE123600

Zhang et al., iScience *21*, 549–561
November 22, 2019
https://doi.org/10.1016/j.isci.2019.10.050

iScience

CellPress

Article

Targeted Drug-Loaded Chemical Probe Staining Assay to Predict Therapy Response and Function as an Independent Pathological Marker

Heng Zhang,[1,2,4] Wei-long Zhong,[1,3,4] Bo Sun,[2,4] Guang Yang,[1,4] Yan-rong Liu,[2] Bi-jiao Zhou,[1,2] Xin Chen,[1,2] Xiang-yan Jing,[1] Long-cong Huai,[1] Ning Liu,[1] Zhi-yuan Zhang,[2] Mi-mi Li,[2] Jing-xia Han,[2] Kai-liang Qiao,[1] Jing Meng,[1] Hong-gang Zhou,[1,2,*] Shuang Chen,[2,*] Cheng Yang,[1,2,*] and Tao Sun[1,2,5,*]

SUMMARY

Multi-targeted kinase inhibitors, such as sorafenib, have been used in various malignancies, but their efficacy in clinical applications varies among individuals and lacks pretherapeutic prediction measures. We applied the concept of "click chemistry" to pathological staining and established a drug-loaded probe staining assay. We stained the cells and different types of pathological sections and demonstrated that the assay was reliable. We further verified in cells, cell-derived xenograft model, and clinical level that the staining intensity of the probe could reflect drug sensitivity. The stained samples from 300 patients who suffered from hepatocellular carcinoma and used the sorafenib probe also indicated that staining intensity was closely related to clinical information and could be used as an independent marker without undergoing sorafenib therapy for prognosis. This assay provided new ideas for multi-target drug clinical trials, pre-medication prediction, and pathological research.

INTRODUCTION

Targeted drug therapy is regarded as the main treatment for malignant tumors. Next-generation sequencing (NGS) has been widely used as a clinical diagnostic method for targeted drugs (Khotskaya et al., 2017; Prasad et al., 2016). In lung cancer and breast cancer treatments, tyrosine-kinase inhibitors, a kind of single-target drug, can accurately target a certain kinase or its mutation (Grimminger et al., 2010). A class of targeted drugs exists, and it includes multi-target kinase inhibitors, such as sorafenib (Wilhelm et al., 2006), which is the first drug approved for the treatment of advanced hepatocellular carcinoma (HCC) (Raoul et al., 2018). This class of drugs cannot rely on NGS for premedication diagnosis. Accurately predicting a target's level in clinical trials during drug development is also difficult (Llovet et al., 2008). In clinical applications, the therapeutic effects of multi-target drugs often vary among individuals, and their therapeutic effects are unstable and random, which are similar to traditional chemotherapy (Garraway and Hahn, 2010). Consequently, they become a problem in the clinical use of targeted drugs. The efficacy and adaptation of a population can be confirmed through large multi-center clinical trials or meta-analysis. For instance, sorafenib can inhibit up to 40 kinases, including angiogenic receptor tyrosine kinases (RTKs), such as VEGF receptors (VEGFRs) and PDGF receptor-β (PDGFRβ), and play a role in anti-angiogenesis and antitumor proliferation (Wilhelm et al., 2008). Biomarkers capable of predicting sorafenib reactivity have yet to be discovered because of the diversity and pharmacological complexity of sorafenib targets. Although patient-derived tumor xenografts (PDTX) can be used to predict drug sensitivity, this method is time consuming, costly, and difficult to use universally. NGS is also difficult to predict the therapy response of these drugs (Tentler et al., 2012). Therefore, efficient methods should be developed to predict whether a patient can respond to multi-target drugs and guide clinical use (Llovet et al., 2018).

On the basis of our previous work (Zhong et al., 2016), we introduced a pathological staining assay by using a targeted drug-loaded probe based on chemical probes used for drug target research. The assay could evaluate the subcellular location and relative expression of a drug target in a surgical resection tissue or a biopsy specimen in a short period and predict the reaction of patients to a drug. The assay was independent of NGS and could be compared with pathological immunohistochemistry and H&E staining for an effective coordination.

[1]State Key Laboratory of Medicinal Chemical Biology and College of Pharmacy, Nankai University, Tianjin, China

[2]Tianjin Key Laboratory of Early Druggability Evaluation of Innovative Drugs and Tianjin Key Laboratory of Molecular Drug Research, Tianjin International Joint Academy of Biomedicine, Tianjin, China

[3]Department of Gastroenterology and Hepatology, Tianjin Medical University General Hospital, Tianjin Institute of Digestive Disease, Tianjin, China

[4]These authors contributed equally

[5]Lead Contact

*Correspondence: honggang.zhou@nankai.edu.cn (H.-g.Z.), shuang7332@163.com (S.C.), cheng.yang@nankai.edu.cn (C.Y.), tao.sun@nankai.edu.cn (T.S.)

https://doi.org/10.1016/j.isci.2019.10.050

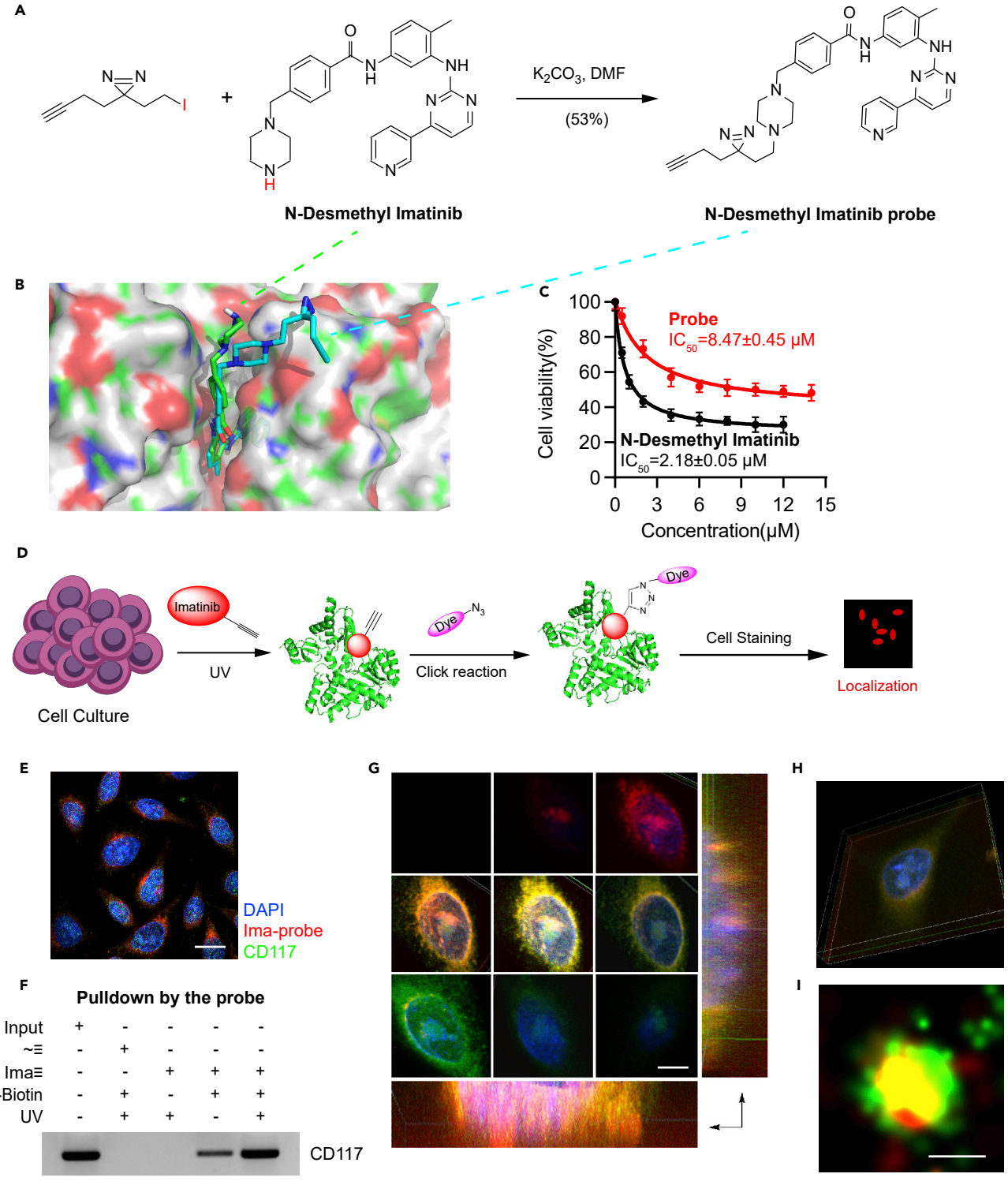

Figure 1. Imatinib Probe Could Bind to CD117

(A) Chemical synthesis route of imatinib probe.

(B) Imatinib and probes were docked with CD117 protein.

(C) Effect of imatinib and probe on proliferation of GIST882 cell line. Each bar represents the mean ± SD for triplicate experiments.

(D) Schematic diagram of cell staining with imatinib probe.

(E) Simultaneous staining with imatinib probe and CD117 immunofluorescence staining on the GIST882 cell line, scale bar = 10 μm.

Figure 1. *Continued*

(F) Target was captured on the GIST882 cell line using N_3-biotin and probe in combination with pulldown and detected using Western blot analysis of CD117.

(G) Imatinib probe staining and CD117 immunofluorescence staining, z axis sweep with confocal microscopy, scale bar = 5 μm.

(H) Three-dimensional reconstruction of Figure 1G after sweeping.

(I) Co-localization of imatinib probe staining and CD117 immunofluorescence in single molecule levels observed using a super resolution microscope, scale bar = 0.1 μm.

The term "click chemistry" was first fully described by Sharpless in 2001 (Kolb et al., 2001) and has been widely used in biochemical labeling (Meghani et al., 2017; Wright and Sieber, 2016). The classic click reaction is the copper-catalyzed reaction of an azide with an alkyne to form a five-membered heteroatom ring (Rostovtsev et al., 2002). In this study, we modified the inactive functional group of the original drug molecule with a terminal alkyne as a drug probe to allow minimal functionalization. We added the probe to the test sample, which bound to the target protein, and linked azide-tagged rhodamine to the probe *in vitro* via a click reaction, or a copper-catalyzed azide–alkyne cycloaddition reaction, which enabled fluorescence to represent the characteristics of the drugs. To reduce the probability of a probe off-target and increase the binding force and sensitivity of the probe and the drug, we introduced the light affinity group (double acridine) to the probe under ultraviolet (UV) exposure. The group could combine with the amino acid near the drug pocket to form covalent binding so that the probe and the target protein bind more closely (Li and Zhang, 2016).

To test the feasibility of this assay, we used a classic target drug, namely, single-target imatinib, to establish the probe staining assay combined with IF of its target CD117 and other methods and evaluate the reliability of the proposed method on gastrointestinal stromal tumor (GIST) (Joensuu et al., 2013). Our results showed that the assay worked. We also designed the multi-target drug sorafenib probe and applied it to predict drug reactivity (sensitivity) in HCC and confirm targets. Probe staining result suggested that sorafenib staining positive cluster could be used as an independent prognostic indicator for pathological diagnosis.

RESULTS

Imatinib Probe Could Bind to CD117

On the basis of the structure–activity relationship of imatinib, we determined that the probe-modified position was a nonpocket-binding functional base (Manley et al., 2010). Therefore, the synthetic route shown in Figure 1A was designed, the imatinib probe was obtained, and the structure was confirmed through nuclear magnetic resonance (NMR) (Figure S1). The probe was studied in terms of its ability to bind well to a target because its structure differed from that of the original drug. We first evaluated whether the activity of the probe was similar to that of the original drug. Using the computer docking program, we docked imatinib (green) and the probe (blue) with their target CD117. In Figure 1B, the conformation of the two combined with the CD117 active pocket was similar, and the probe-modified group was on the outer side of the active pocket. We further used surface plasmon resonance (SPR) to investigate the binding affinity of imatinib and the probe to CD117. As shown in Figure S2, binding of imatinib and the probe to CD117 was dose dependent, exhibiting a fast association-dissociation process. The response units at equilibrium were plotted against imatinib and the probe concentrations, and the dissociation constant (KD) was calculated by non-linear regression, suggesting that the binding affinity of imatinib and the probe to CD117 was similar. Conducting the CCK-8 assay, we tested the effect of imatinib and its probe on the proliferation of the imatinib-sensitive gastrointestinal stromal tumor cell line GIST882. In Figure 1C, the curves of imatinib and imatinib-probe were similar in shape with IC_{50} of 2.18 and 8.47 μM, indicating that the activity of the two cells had the same order of magnitude. Next, we stained the cells with the imatinib probe by applying the procedure shown in Figure 1D and observed the colocalization of the CD117 fluorescence (Figure 1E). We also used confocal three-dimensional layer sweep (Figures 1G) and 3D reconstruction (Figure 1H) to demonstrate that probe staining was colocalized with CD117 on the membrane. Super-resolution microscopy revealed that they combined well with high specificity in a single molecule level (Figure 1I). Pearson correlation coefficient (PCC) was 0.744, and Mander's overlap coefficient (MOC) was 0.759. We also used the imatinib probe pulldown to confirm that CD117 was detected through Western blot analysis (Figure 1F). These results indicated that the probe could bind to the target of the original drug and produce a similar inhibitory activity.

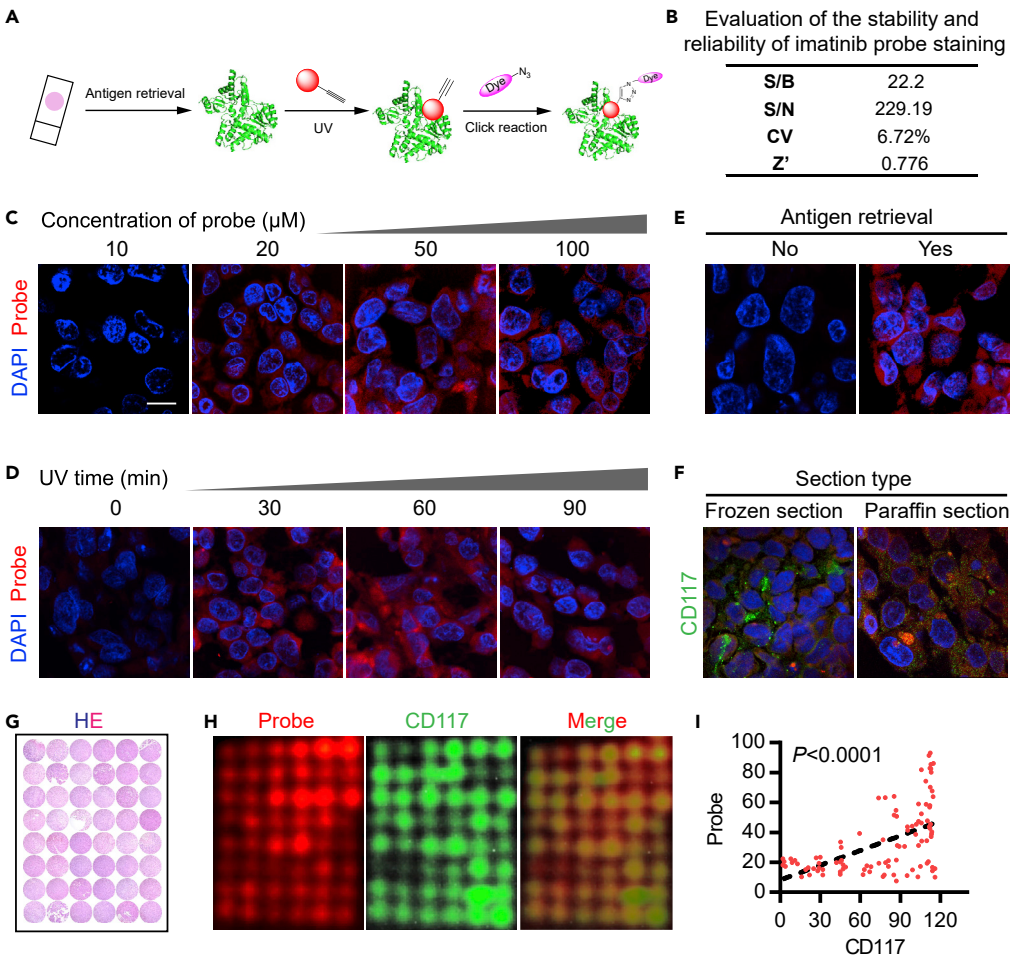

Figure 2. Establishment of Pathological Section Staining Process Using Imatinib Probe

(A) Procedure for staining the imatinib probe on tissue sections.

(B) Evaluation of imatinib probe stability and reliability.

(C–E) Staining results obtained under different conditions: the concentration of the probe (C), the time of UV exposure (D), and antigen retrieval (E), scale bar = 10 μm.

(F) Imatinib probe staining and CD117 immunofluorescence staining on frozen sections and paraffin sections.

(G) HE staining of the GIST tissue microarray.

(H) Staining with the imatinib probe (red) and CD117 immunofluorescence staining (green) on the GIST tissue microarray.

(I) Correlation analysis of probe staining and CD117 staining on the GIST tissue microarray.

Establishment of Pathological Section Staining by Using the Imatinib Probe

We stained the pathological sections in accordance with the procedure shown in Figure 2A and evaluated the stability and reliability of staining (Figure 2B). The Z factor of staining was 0.776, and the coefficient of variation (CV) was 6.72%. We explored the following conditions of the key steps: the concentration of the probe (Figure 2C), the time of UV exposure (Figure 2D), and antigen retrieval (Figure 2E). We found that microwave antigen retrieval could be achieved in the paraffin sections of the conventional formalin-fixed specimens at a probe concentration of 50 μM and a UV exposure duration of 60 min. On the basis of these experimental conditions, we compared the staining effects on frozen sections and paraffin sections. The comparison with CD117 immunofluorescence showed that they had fine colocalization (Figure 2F). The frozen sections could be stained without antigen retrieval, and the paraffin sections were more suitable than the frozen sections for antigen retrieval. On the basis of these findings, we collected 24 pathological paraffin specimens of gastrointestinal stromal tumors from well-diagnosed patients in clinical and fabricated tissue microarrays (HE staining image shown in Figure 2G) to meet the fluorescence analysis requirement under the same conditions. Probe staining and immunofluorescence on the tissue chip were similar

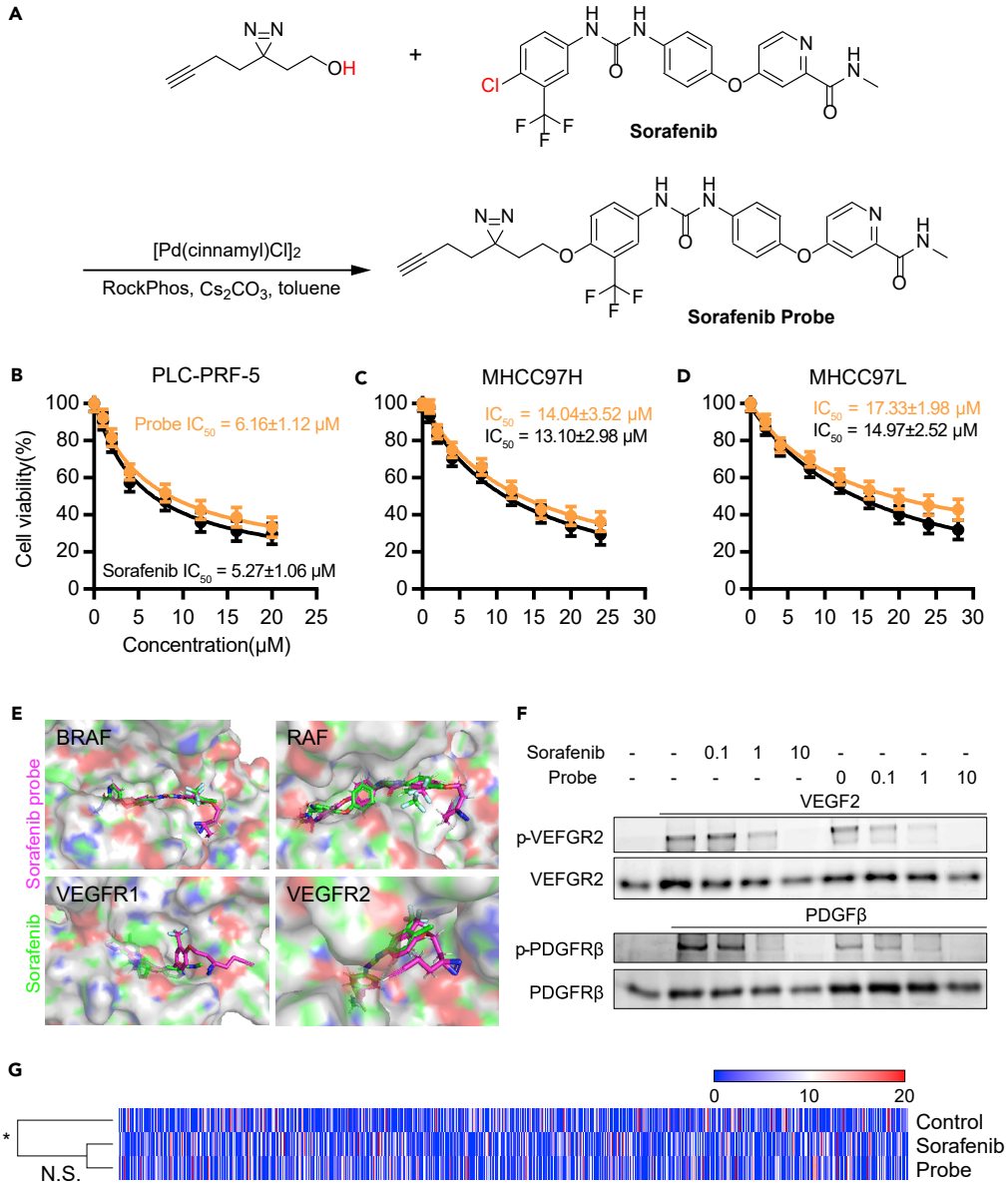

Figure 3. Preparation of Sorafenib Probe for Fluorescence Staining

(A) Chemical synthesis route of sorafenib probe.

(B–D) Effects of different concentrations of sorafenib and probe on the proliferation of PLC-PRF-5 (B), MHCC97H (C), and MHCC97L (D) cell lines. Each bar represents the mean ± SD for triplicate experiments.

(E) Sorafenib and probes were mock docked with four known targets of sorafenib.

(F) Effects of different concentrations of sorafenib and probe on the expression of VEGFR2, PDGFRβ, and phosphorylation at the target.

(G) Expression profiles of the PLC-PRF-5 cell lines treated with solvent, sorafenib, and probe are not significantly different between the sorafenib and probe groups, and the solvent group was significantly different from the two other groups.

to those on the cells and had a fine colocalization effect (Figure 2H); MOC was 0.904 and PCC was 0.711. The staining intensity of the probe was significantly correlated with the CD117 fluorescence intensity ($p < 0.0001$; Figure 2I), suggesting that the probe staining assay was effective.

Preparation of Sorafenib Probe for Fluorescence Staining

After confirming the feasibility of the staining method with the single-target drug imatinib probe, we synthesized the sorafenib probe by following the synthetic route shown in Figure 3A to study if the previously

described assay could solve targeted drug-related problems to some extent. On the basis of the structure–activity relationship of imatinib, According to the structure–activity relationship of sorafenib, we determined that the probe-modified position was not the binding functional base (Ramurthy et al., 2008). The probe was briefly described using several steps of synthesis, and its structure was characterized using NMR (Figure S3). We first evaluated whether the activity of the probe was similar to the activity of the original drug by applying the methods that we used for the imatinib probe. Using the CCK-8 assay, we tested the effects of sorafenib and the probe on the proliferation of HCC cell-lines PLC-PRF-5 (Figure 3B), MHCC97H (Figure 3C), and MHCC97L (Figure 3D). The results showed that sorafenib and the probe had similar IC_{50} in the three cell lines, indicating that both had similar effects on cell proliferation. Sorafenib (green) and the probe (purple) were docked with the known targets BRAF, RAF, VEGFR1, and VEGFR2 by using the computer docking program. In Figure 3E, the conformation of the binding of sorafenib and the probe to the active pockets of these targets was similar, and the terminal alkyne portion of the probe was located outside the active pocket. As shown in Figure S4, binding of sorafenib and the probe to VEGFR1 and VEGFR2 was dose dependent, exhibiting a fast association-dissociation process. The response units at equilibrium were plotted against sorafenib and the probe concentrations, and the dissociation constant (KD) was calculated by non-linear regression, suggesting that the binding affinity of sorafenib and the probe to VEGFR1 and VEGFR2 was similar. We performed Western blot analysis to detect the phosphorylation and expression of VEGFR2 and PDGFR-β in the PLC-PRF-5 cell line. The results showed that VEGFR2 phosphorylation in sorafenib and sorafenib probe treatment groups were dose-dependently reduced (Figure 3F), whereas the total amount did not change significantly. PDGFR-β phosphorylation was dose-dependently reduced, and the total amount was not significantly changed. These results indicated that the inhibitory effects of the original drug and the probe on the activity of the two targets were similar. We also used an expression profiling chip to detect the expression profile of PLC-PRF-5 cells after they were treated with sorafenib and its probe (Figure 3G). The effects of the two substances on cell expression profiles were similar, and the clustering results were not significant. The drug and probe groups were categorized into one class, and the solvent was classified into another one. These results suggested that the binding target of the sorafenib probe was consistent with that of sorafenib.

Sorafenib Probe Staining Intensity Was Related to Drug Sensitivity

We selected 10 cell lines and stained them with sorafenib probe. The images of PLC-PRF-5, Huh7, MHCC97H, and MHCC97L staining are presented in Figure 4A. The stability and reliability of probe staining were evaluated using the factors shown in Figure 4B. IC_{50} of sorafenib was also tested with CCK-8 in these cell lines. The results showed that sorafenib probe staining intensity was negatively correlated with IC_{50} ($p < 0.0001$; Figure 4C), indicating that probe staining represented drug sensitivity. We then used these 10 cell lines to establish cell-derived xenograft models and study their sensitivity to sorafenib treatment. Consistent with the cell experiment, the models demonstrated that the tumor inhibition rate of sorafenib was positively correlated with staining intensity in different cell lines (Figure 4D). We collected pathological sections of 34 patients (Table S3) who suffered from HCC and underwent sorafenib therapy after surgery and prospectively analyzed the relationship between probe staining intensity and drug efficacy. In Figure 4E, PFS increased in the three groups of patients with weak, medium, and strong probe staining ($p < 0.0001$), indicating that patients with strong staining were more sensitive to sorafenib treatment. On the basis of the sensitivity of the 34 patients to sorafenib as predicted by the sorafenib probe, we plotted the receiver operating characteristic (ROC) curve (Figure 4F) with an area under the curve (AUC) of 0.775, indicating that the probe staining intensity was a good predictor of drug sensitivity. These results suggested that sorafenib probe staining could reflect the drug sensitivity of sorafenib in cells, cell xenografts, and clinical levels and that probe staining could be used on surgical specimens to predict postoperative drug use.

Meta-Analysis Showed Sorafenib Had Different Effects on Various Populations

Considering that probe staining could effectively predict the efficacy of a drug, we further determined whether probe staining could also be used for the prognostic evaluation of clinical cases or whether the effect of a drug on prognosis could be understood by slice staining before treatment to enrich the detection range of pathological diagnosis. We used the sorafenib probe to establish a predictive assay independent of treatment and targets. First, we tested whether the drug treatment of sorafenib could affect survival time to verify whether the drug was useful. Numerous clinical multicenter studies on sorafenib have been performed, but no conclusive evidence-based medical certificate has been provided. As such, we used the flow chart shown in Figure S5A for meta-analysis. We then retrieved and included five

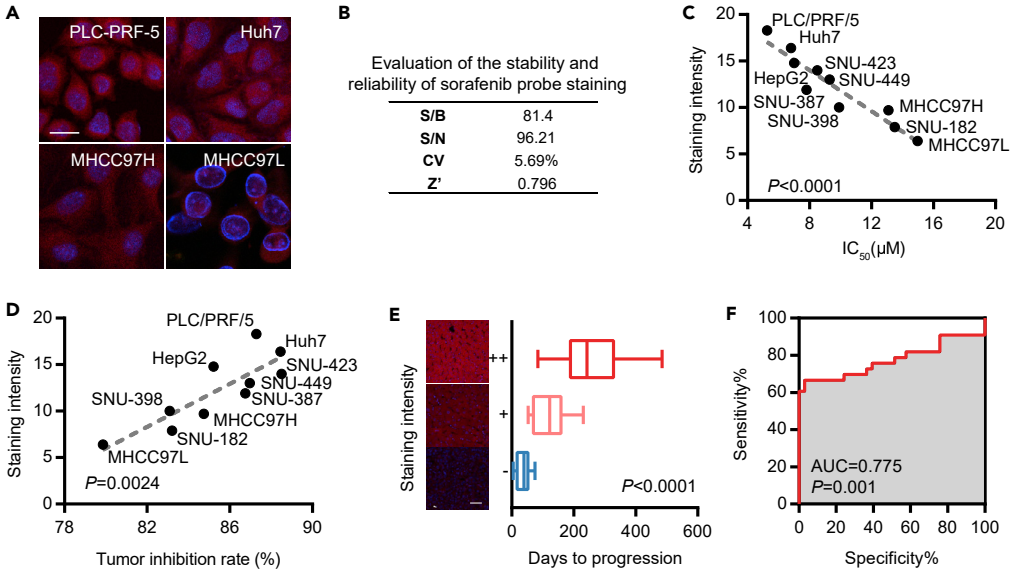

Figure 4. Sorafenib Probe Staining Intensity Was Related to Drug Sensitivity

(A) Sorafenib probe was used to stain PLC-PRF-5, Huh7, MHCC97H, and MHCC97L cell lines; red = probe, blue = DAPI, scale bar = 15 μm.

(B) Evaluation of sorafenib probe stability and reliability.

(C) The staining intensity of 10 cell lines and the regression analysis of sorafenib IC_{50} showed a negative correlation.

(D) After establishing cell-derived xenograft model of 10 cell lines, a positive correlation was found between tumor inhibition rate and staining intensity after treatment with sorafenib.

(E) The 33 patients given with sorafenib after surgery were stained with the probe, and the PFS of strongly positive, weakly positive, and negative groups (representative results on the left, scale bar = 50 μm) was successively decreased.

(F) ROC curve of sorafenib probe's prediction of sorafenib sensitivity in 33 patients.

articles, and the basic information is shown in Table S4. Meta-analysis indicated that the overall survival [OS] of patients treated with sorafenib increased (hazard ratio [HR] = 0.69, 95% confidence interval [CI] 0.57–0.82; Figure S5B) compared with that of patients administered with placebo, and various effects were observed in different case groups (Table S5). The effects of sorafenib treatment on patients with extra-hepatic metastasis and hepatitis B infection were not evident. In other subgroups, such as ECOG PS, vascular invasion, and hepatitis C infection groups, sorafenib exhibited significant efficacy ($p < 0.05$). Sorafenib also improved OS (Figure S5C) compared with that of other targeted drugs (HR = 0.88, 95% CI 0.81–0.95) and elicited various effects on different case groups (Table S6). In comparison with other targeted drugs, sorafenib significantly improved the OS of Asian populations and patients with hepatitis C infection ($p < 0.05$).

Sorafenib Targets Were Complex and Closely Related to the Prognosis of HCC

The improvement of the survival of patients with HCC and the various effects of sorafenib on different cases indicated that the target group was closely related to the prognosis of HCC, and the overall expression of these target groups differed among patients. We used the probe to capture the sorafenib target (Figure 5A). The gel was run, and Coomassie blue staining (Figure 5B), enzymatic digestion, and identification via bio-mass spectrometry were performed. We comprehensively analyzed the target results obtained via pulldown, the sorafenib target contained in the Drugbank database (Wishart et al., 2018), and the prediction results obtained using online target prediction tools, namely, SEA (Keiser et al., 2007), SwissTargetPrediction (Gfeller et al., 2014) and BATMAN (Liu et al., 2016). The three sets of targets were shown in Figure 5C; many targets have not been reported, for example, TTK, KRT8, and CCDC22. The GSEA analysis after Huh7 cell line was treated with sorafenib (Won et al., 2017) validated the rationality of the obtained potential targets (Figure 5D). We analyzed some potential targets, KIT, RAF1, KRT8, and TTK by using HCC data in TCGA (Figures 5E–5G). The results showed that the high expression levels of KIT, RAF1, KRT8, and TTK were indicative of poor prognosis of HCC and were related to grade and stage. Some target expression levels had no significant relationship with the prognosis, grade, and stage of HCC (Figure S6). Sorafenib targets were complicated, but they were related to the prognosis of HCC as a

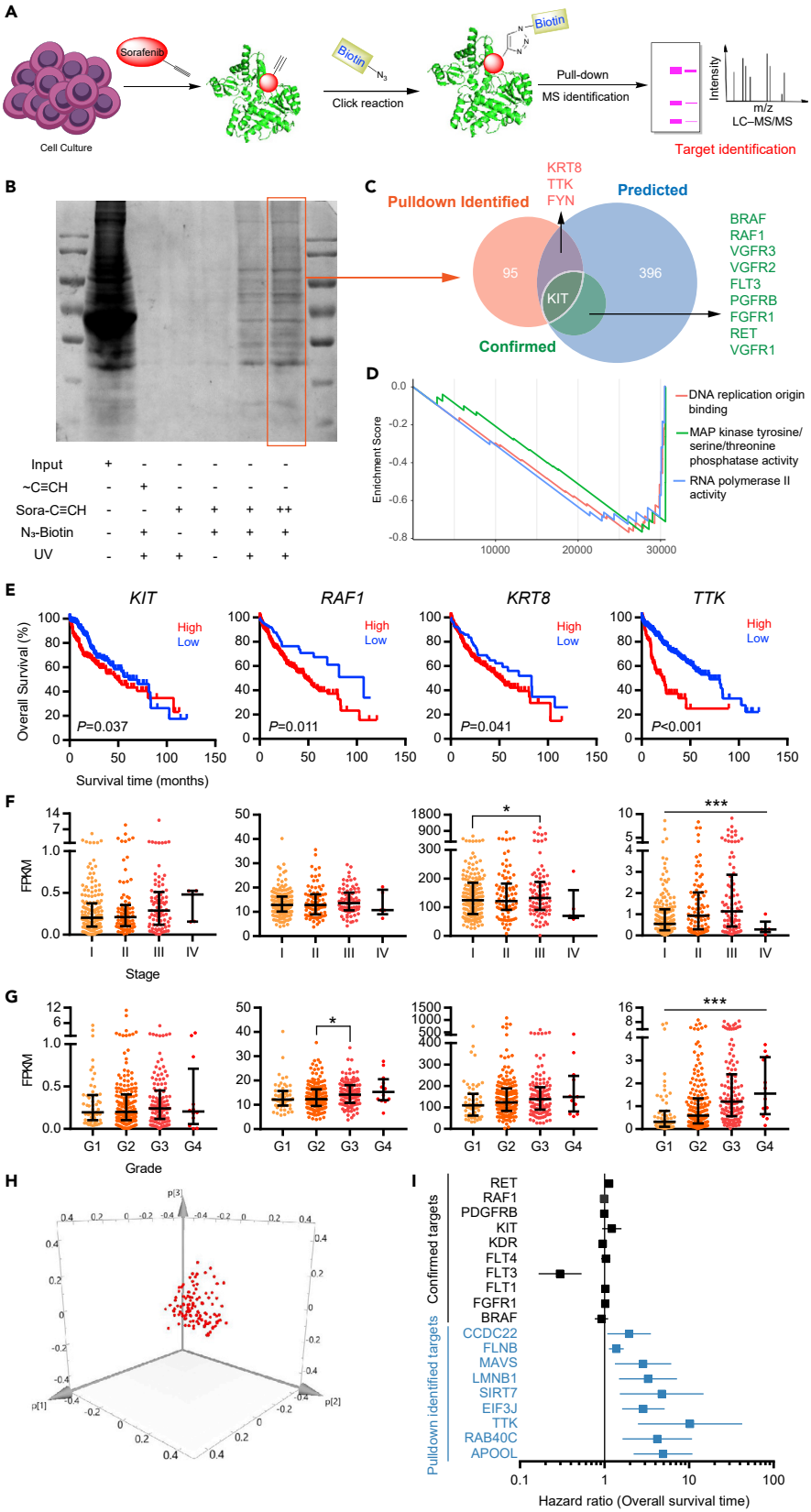
A
Sorafenib
Cell Culture
Biotin
Click reaction
Pull-down
MS identification
Intensity
m/z
LC–MS/MS
Target identification
B
Input
~C≡CH
Sora-C≡CH
N3-Biotin
UV
C
Pulldown Identified
Predicted
KRT8
TTK
FYN
95
396
KIT
Confirmed
BRAF
RAF1
VGFR3
VGFR2
FLT3
PGFRB
FGFR1
RET
VGFR1
D
Enrichment Score
DNA replication origin binding
MAP kinase tyrosine/serine/threonine phosphatase activity
RNA polymerase II activity
E
KIT
RAF1
KRT8
TTK
High
Low
Overall Survival (%)
P=0.037
P=0.011
P=0.041
P<0.001
Survival time (months)
F
FPKM
Stage
G
Grade
H
I
Confirmed targets
Pulldown identified targets
RET
RAF1
PDGFRB
KIT
KDR
FLT4
FLT3
FLT1
FGFR1
BRAF
CCDC22
FLNB
MAVS
LMNB1
SIRT7
EIF3J
TTK
RAB40C
APOOL
Hazard ratio (Overall survival time)

Figure 5. Sorafenib Targets Were Complex and Closely Related to the Prognosis of HCC

(A) Schematic of fishing targets with the sorafenib probe.

(B) Coomassie blue staining of the proteins after pulldown with the sorafenib probe.

(C) Venn diagram of sorafenib-known targets, online predicted targets, and pulldown targets.

(D) GSEA analysis after treatment of the Huh7 cell line with sorafenib.

(E–G) TCGA data showed that sorafenib's known targets, namely, KIT, RAF1, fishing target KRT8, and TTK are related to HCC overall survival (E), stage (F), and grade (G). *$p < 0.05$, ***$p < 0.001$.

(H) PCA analysis of known and potential targets of sorafenib.

(I) COX regression survival analysis of known target and fishing target of sorafenib.

whole function. Thus, the target group could be regarded as a cluster. We performed PCA on these targets by using TCGA RNA-seq data (Figure 5H) and showed that the expression of these targets was clustered. COX regression analysis revealed that the reported targets slightly contributed to prognosis, whereas the potential targets TTK, CCDC22, and SIRT7 had a high risk of prognosis of HCC (Figure 5I). Thus, the real target of sorafenib should be further studied.

Sorafenib Target Cluster Stained Using the Sorafenib Probe Could Be Used as an Independent Prognostic Marker of HCC

Meta-analysis indicated that sorafenib treatment could improve the survival time of patients, especially in the absence of extrahepatic metastasis, vascular invasion, and other remarkable indicators. We also used biochemical methods to identify sorafenib targets, and many of these targets affect prognosis and clinicopathological parameters. Therefore, we aimed to establish a sorafenib probe stain as a novel and independent pathological stain marker for clinical prognosis evaluation. Pathological tissues stained with a sorafenib-loaded probe were not obtained from patients who took sorafenib. The staining results indicated the total expression level of sorafenib targets. We defined the expression of this total target group as ''sorafenib probe cluster'', which was unrelated to the intake or non-intake of sorafenib.

We collected 75 cases of HCC specimens with complete clinical information (Table S7) and prepared a tissue microarray. The specimens were collected from patients who did not take sorafenib and used for retrospective clinicopathological studies on probe fluorescent staining. The results of tissue microarray HE staining and fluorescence staining are shown in Figure 6A. High-magnification images of different staining intensities are shown in Figures 6B and S8. The HE staining, hepatocyte staining, and probe staining results of the same sample are illustrated in Figure 6C, indicating that the probe can be accurately positioned in the parenchyma rather than in the stroma. We analyzed staining intensity and clinical information and demonstrated that staining intensity was not significantly different in terms of gender and age (Figure S7) but was positively correlated with clinical stage (Figure 6D, $p = 0.0388$), T stage (Figure 6E, $p = 0.0227$), N stage (Figure 6F, $p = 0.0369$), and grade (Figure 6G, $p = 0.0476$). The staining results were negatively correlated with HBV status (Figure 6H, $p = 0.0483$), AFP (Figure 6I, $p = 0.0376$), and CEA level (Figure 6J, $p = 0.0387$). The KM survival analysis of staining intensity (Figure 6K) showed that the survival of the patients with strong positive staining was significantly shorter than that of the patients with weak positive and negative staining. The median survival periods of the three groups were 28, 68, and 87 days ($p = 0.0031$). We also performed immunohistochemical staining for the three sorafenib targets, namely, VEGFR1, VEGFR2, and PDGFRβ, by using the tissue microarray of the same sample and conducted correlation analysis between staining intensity and immunohistochemical score. The results showed that the staining intensity was positively correlated with the immunohistochemical scores of the three targets. Pearson correlation coefficients were 0.4158 (Figure 6L), 0.2512 (Figure 6M), and 0.2432 (Figure 6N) ($p < 0.05$). Representative images are shown in Figures 6O–6Q. We combined the immunohistochemical results of VEGFR1 and VEGFR2 with the sorafenib probe staining results of HCC and adjacent tissues and found that the sorafenib probe stained the blood vessels (Figure S8F green arrow; Figure S8G arrow) but did not stain the bile duct (Figure 6O green arrow and Figure S8F yellow arrow).

Sorafenib probe staining could be used not only to diagnose tumor cells but also to label stroma and reactive vessels. These results indicated that sorafenib probe staining corresponded to the expression level of total targets of sorafenib with poor prognosis and was associated with clinical stage and pathological grade. Reactive stroma and vascular invasion are markers of the poor prognosis of HCC and the main target tissue of sorafenib. The results of probe staining were consistent with the results of drug efficacy meta-analysis. Therefore, sorafenib probe cluster staining could be used as an independent prognostic marker and was independent of sorafenib treatment.

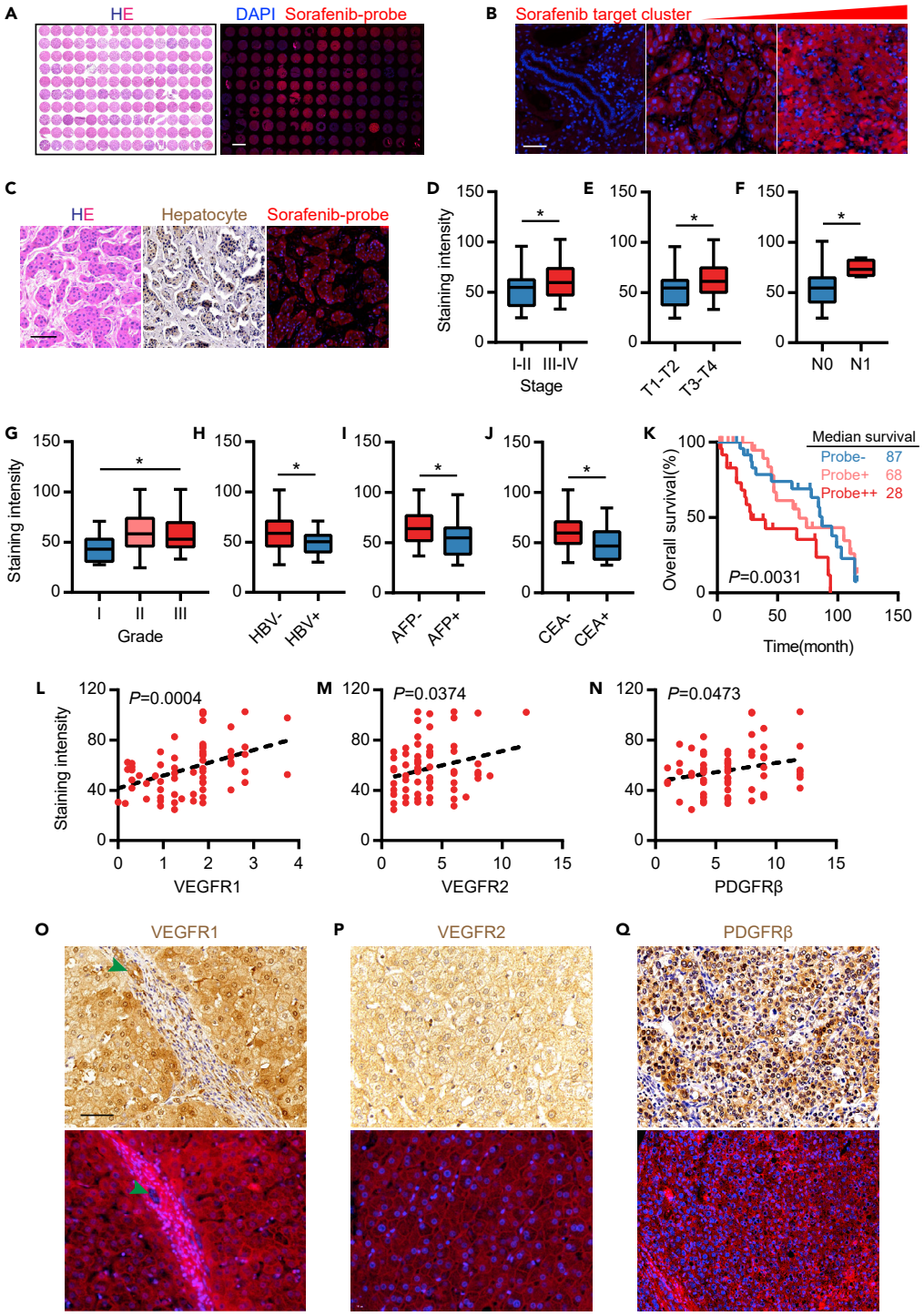

Figure 6. Sorafenib Target Cluster Stained with Sorafenib Probe Could Be Used as an Independent Prognosis Marker for HCC

(A) HCC tissue chip HE staining and sorafenib probe staining results, scale bar = 2 cm.

(B) High magnification image of sorafenib probe staining (negative, weakly positive, and strong positive), scale bar = 50 μm.

(C) HE staining, hepatocyte staining, and probe staining of the same tissue.

(D–J) Relationship between staining intensity and clinical stage (D), T stage (E), N stage (F), grade (G), HBV state (H), AFP (I), and CEA level (J). *p < 0.05.

Figure 6. *Continued*

(K) KM survival analysis of strong positive, weak positive, and negative groups according to the intensity of staining.

(L–N) Correlation analysis of sorafenib probe staining intensity with the three targets, namely, VEGFR1 (L), VEGFR2 (M), and PDGFRβ (N) immunohistochemical scores.

(O) VEGFR1 immunohistochemical (top) and probe staining (bottom) results for the same sample with the green arrow indicating bile duct, scale bar = 50 μm.

(P) VEGFR2 immunohistochemistry (top) and probe staining (bottom) in the same sample.

(Q) PDGFRβ immunohistochemical (top) and probe staining (bottom) results for the same sample.

DISCUSSION

Drug-loaded chemical probe staining assays on pathological sections have a completely different principle from traditional chemical staining and immunohistochemical staining in pathology and are an important addition to classical pathological diagnostic techniques. In this study, the proposed assay applies click chemistry in which a fluorophore is introduced into a drug probe after it binds to a target protein to achieve fluorescent staining. As such, this assay may become an important component of immunohistochemical staining in pathology and promote the use of small-molecule drugs for pathological section staining. For example, the results of sorafenib probe staining could predict its efficacy and address NGS defects on multi-targeted drugs. The results of probe staining were also closely related to clinical pathological information and could be used as an independent pathological marker. This finding suggested that small-molecule drugs could also be transformed into probes that could be used by pathologists to study various pathological phenomena and observe the population expression levels of multiple targets.

When we used the sorafenib probe to study its target and staining, we found that its known target slightly contributed to the prognosis of HCC, but many potential targets had a high risk ratio for HCC prognosis. Thus, we proposed the concept of "drug target cluster," which referred to total targets of a drug. Drug target cluster can be visualized by the drug-loaded probe staining assay. For a targeted drug, drug target cluster was fixed, and the staining intensity of different patient samples could be obtained through the assay. The expression level of a patient's drug target cluster could be summarized as follows: the stronger the staining, the higher the total target expression of the drug and better the expected therapeutic effect of the drug would be. Conversely, the weaker the staining, the lesser the total target expression of the drug would be in the corresponding part of the patient. Thus, the worse outcome of the effect of the targeted drug treatment was expected. This finding might help doctors determine a patient's drug sensitivity to a certain extent, that is, whether a drug was suitable for targeted drug treatment. NGS is currently recognized as a probable therapeutic predictor for single-targeted drugs and applicable to immunotherapy, but NGS is almost useless for multi-targeted drugs. Evaluating currently unknown drug targets using NGS is also impossible. Many single-target drugs also have multiple sub-targets, which often lead to missed drug use opportunities for sensitive patients. At the same time, if an epigenetic change occurs in the target of a single-target drug, this drug cannot combine with it. Although NGS shows the target is positive in a patient, the drug often appears to be ineffective. Therefore, NGS use is uncertain even for single-target drugs. The staining assay proposed in this paper could effectively assist NGS for predicting the effect of drug treatments.

Probe staining can be used not only as a predictive marker for treatment but also as an independent prognostic marker. Targeted drugs work because "drug target cluster" has a poor prognosis as a whole. After the targets are inhibited by the drug, the survival time of a patient can be improved. This observation also supports the clinical feasibility of sorafenib. Drug probe staining can indicate some pathological phenomena, including labeled reactive stroma in tumors, invaded vessels in tumors, and presence of staining signals in the nucleus. Further research is needed to determine why drug target cluster is positively associated with these pathological phenomena. Besides, active small molecules can be used not only as drugs but also as independent clinical pathological markers for specific mechanism research and clinical diagnosis. This assay would become a new type of chemical staining technology named "drug binding histochemical staining (DHC)."

When we established this staining assay, we optimized many conditions. For instance, in pathological section staining, we suggested adding a negative control and a positive control to the sample to rule out fluctuations in staining conditions, in order to reduce the probability of false negative or false positive. For this reason, we used pathological tissue microarrays to evaluate imatinib probe staining with target colocalization and the relationship of the staining intensity of sorafenib probe to clinical information to ensure that the staining conditions were identical, and the results were comparable.

A drug-loaded probe staining assay is established to reflect the drug sensitivity of sorafenib in cells, animals, and humans. Sorafenib probe staining is also associated with clinical information and pathological phenomena and thus considered an independent pathological marker. This finding may help solve the clinical problem of targeted drug sensitivity prediction and provide new ideas for the pathological diagnosis of HCC and other pathological phenomena.

Limitations of the Study

The probe adds a terminal alkyne group and a photoaffinity group to the original drug molecule. Despite this relatively slight modification, the effect is hardly the same as the original drug, and a small portion of the probe may be combined with a nontarget protein. More sophisticated probes that are similar to the original drug structure should be further designed to improve staining specificity. This idea should also be applied to develop more probes for targeted drugs and verify the reliability and universality of the assay.

METHODS

All methods can be found in the accompanying Transparent Methods supplemental file.

DATA AND CODE AVAILABILITY

The accession number for the data reported in this paper is GEO: GSE123600.

SUPPLEMENTAL INFORMATION

Supplemental Information can be found online at https://doi.org/10.1016/j.isci.2019.10.050.

ACKNOWLEDGMENTS

This study was supported by the National Natural Science Foundation of China (grant no. 81972629, 81972746 and 8197111486), National New Drug Creation Special Project of China (grant no. 2018ZX09736-005) and Tianjin Science and Technology Project (grant no. 18PTSYJC00060).

AUTHOR CONTRIBUTIONS

Heng Zhang and Weilong Zhong carried out experiments, analyzed data, drafted the manuscript, and edited figures. Bo Sun, Guang Yang, Bijiao Zhou, Xiangyan Jing, Xin Chen, and Longcong Huai carried out experiments. Yanrong Liu and Ning Liu carried out experiments, analyzed data, and provided technical support. Zhiyuan Zhang, Mimi Li, Jingxia Han, Kailiang Qiao, Jing Meng, and Shuang Chen provided technical support. Honggang Zhou and Cheng Yang secured funding. Tao Sun conceived experiments, edited the manuscript and figures, and secured funding. All authors had final approval of the submitted and published versions of the manuscript.

DECLARATION OF INTERESTS

The authors declare that they have no conflicts of interest.

Received: June 13, 2019
Revised: October 22, 2019
Accepted: October 24, 2019
Published: November 22, 2019

REFERENCES

Garraway, L.A., and Hahn, W.C. (2010). On or off target: mutations, models, and predictions. Sci. Transl. Med. *2*, 35ps28.

Gfeller, D., Grosdidier, A., Wirth, M., Daina, A., Michielin, O., and Zoete, V. (2014). SwissTargetPrediction: a web server for target prediction of bioactive small molecules. Nucleic Acids Res. *42*, W32–W38.

Grimminger, F., Schermuly, R.T., and Ghofrani, H.A. (2010). Targeting non-malignant disorders with tyrosine kinase inhibitors. Nat. Rev. Drug Discov. *9*, 956–970.

Joensuu, H., Hohenberger, P., and Corless, C.L. (2013). Gastrointestinal stromal tumour. Lancet *382*, 973–983.

Keiser, M.J., Roth, B.L., Armbruster, B.N., Ernsberger, P., Irwin, J.J., and Shoichet, B.K. (2007). Relating protein pharmacology by ligand chemistry. Nat. Biotechnol. *25*, 197–206.

Khotskaya, Y.B., Mills, G.B., and Mills Shaw, K.R. (2017). Next-generation sequencing and result interpretation in clinical oncology: challenges of personalized cancer therapy. Annu. Rev. Med. *68*, 113–125.

Kolb, H.C., Finn, M.G., and Sharpless, K.B. (2001). Click chemistry: diverse chemical function from a

few good reactions. Angew. Chem. Int. Ed. *40*, 2004–2021.

Li, L., and Zhang, Z. (2016). Development and applications of the copper-catalyzed azide-alkyne cycloaddition (CuAAC) as a bioorthogonal reaction. Molecules *21*, https://doi.org/10.3390/molecules21101393.

Liu, Z., Guo, F., Wang, Y., Li, C., Zhang, X., Li, H., Diao, L., Gu, J., Wang, W., Li, D., et al. (2016). BATMAN-TCM: a bioinformatics analysis tool for molecular mechANism of traditional Chinese medicine. Sci. Rep. *6*, 21146.

Llovet, J.M., Montal, R., Sia, D., and Finn, R.S. (2018). Molecular therapies and precision medicine for hepatocellular carcinoma. Nat. Rev. Clin. Oncol. *15*, 599–616.

Llovet, J.M., Ricci, S., Mazzaferro, V., Hilgard, P., Gane, E., Blanc, J.F., de Oliveira, A.C., Santoro, A., Raoul, J.L., Forner, A., et al. (2008). Sorafenib in advanced hepatocellular carcinoma. N. Engl. J. Med. *359*, 378–390.

Manley, P.W., Stiefl, N., Cowan-Jacob, S.W., Kaufman, S., Mestan, J., Wartmann, M., Wiesmann, M., Woodman, R., and Gallagher, N. (2010). Structural resemblances and comparisons of the relative pharmacological properties of imatinib and nilotinib. Bioorg. Med. Chem. *18*, 6977–6986.

Meghani, N.M., Amin, H.H., and Lee, B.J. (2017). Mechanistic applications of click chemistry for pharmaceutical drug discovery and drug delivery. Drug Discov. Today *22*, 1604–1619.

Prasad, V., Fojo, T., and Brada, M. (2016). Precision oncology: origins, optimism, and potential. Lancet Oncol. *17*, e81–e86.

Ramurthy, S., Subramanian, S., Aikawa, M., Amiri, P., Costales, A., Dove, J., Fong, S., Jansen, J.M., Levine, B., Ma, S., et al. (2008). Design and synthesis of orally bioavailable benzimidazoles as Raf kinase inhibitors. J. Med. Chem. *51*, 7049–7052.

Raoul, J.L., Kudo, M., Finn, R.S., Edeline, J., Reig, M., and Galle, P.R. (2018). Systemic therapy for intermediate and advanced hepatocellular carcinoma: sorafenib and beyond. Cancer Treat. Rev. *68*, 16–24.

Rostovtsev, V.V., Green, L.G., Fokin, V.V., and Sharpless, K.B. (2002). A stepwise huisgen cycloaddition process: copper(I)-catalyzed regioselective "ligation" of azides and terminal alkynes. Angew. Chem. Int. Ed. *41*, 2596–2599.

Tentler, J.J., Tan, A.C., Weekes, C.D., Jimeno, A., Leong, S., Pitts, T.M., Arcaroli, J.J., Messersmith, W.A., and Eckhardt, S.G. (2012). Patient-derived tumour xenografts as models for oncology drug development. Nat. Rev. Clin. Oncol. *9*, 338–350.

Wilhelm, S., Carter, C., Lynch, M., Lowinger, T., Dumas, J., Smith, R.A., Schwartz, B., Simantov, R., and Kelley, S. (2006). Discovery and development of sorafenib: a multikinase inhibitor for treating cancer. Nat. Rev. Drug Discov. *5*, 835–844.

Wilhelm, S.M., Adnane, L., Newell, P., Villanueva, A., Llovet, J.M., and Lynch, M. (2008). Preclinical overview of sorafenib, a multikinase inhibitor that targets both Raf and VEGF and PDGF receptor tyrosine kinase signaling. Mol. Cancer Ther. *7*, 3129–3140.

Wishart, D.S., Feunang, Y.D., Guo, A.C., Lo, E.J., Marcu, A., Grant, J.R., Sajed, T., Johnson, D., Li, C., Sayeeda, Z., et al. (2018). DrugBank 5.0: a major update to the DrugBank database for 2018. Nucleic Acids Res. *46*, D1074–D1082.

Won, J.K., Yu, S.J., Hwang, C.Y., Cho, S.H., Park, S.M., Kim, K., Choi, W.M., Cho, H., Cho, E.J., Lee, J.H., et al. (2017). Protein disulfide isomerase inhibition synergistically enhances the efficacy of sorafenib for hepatocellular carcinoma. Hepatology *66*, 855–868.

Wright, M.H., and Sieber, S.A. (2016). Chemical proteomics approaches for identifying the cellular targets of natural products. Nat. Prod. Rep. *33*, 681–708.

Zhong, W., Sun, B., Lu, C., Yu, H., Wang, C., He, L., Gu, J., Chen, S., Liu, Y., Jing, X., et al. (2016). Problems and solutions in click chemistry applied to drug probes. Sci. Rep. *6*, 35579.

ISCI, Volume *21*

Supplemental Information

Targeted Drug-Loaded Chemical Probe Staining Assay to Predict Therapy Response and Function as an Independent Pathological Marker

Heng Zhang, Wei-long Zhong, Bo Sun, Guang Yang, Yan-rong Liu, Bi-jiao Zhou, Xin Chen, Xiang-yan Jing, Long-cong Huai, Ning Liu, Zhi-yuan Zhang, Mi-mi Li, Jing-xia Han, Kai-liang Qiao, Jing Meng, Hong-gang Zhou, Shuang Chen, Cheng Yang, and Tao Sun

Figure S1. The ^{1}H and ^{13}C NMR spectra of N-Desmethyl imatinib probe

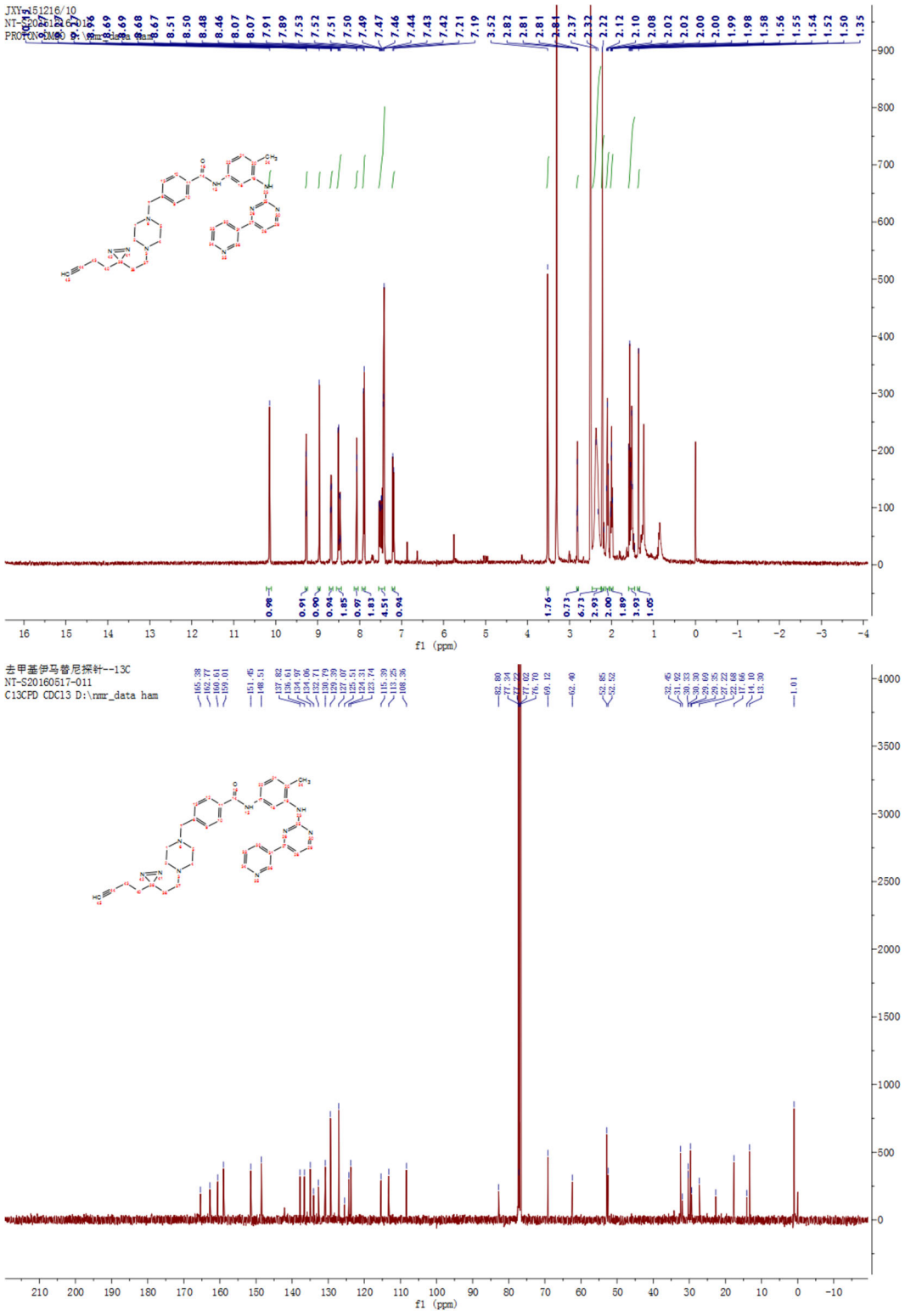

^{1}H NMR (400 MHz, DMSO) δ ppm: 10.15 (s, 1H), 9.30 – 9.24 (m, 1H), 8.96 (s, 1H), 8.68 (dd, J = 4.8, 1.6 Hz, 1H), 8.53 – 8.45 (m, 2H), 8.07 (d, J = 2.1 Hz, 1H), 7.90 (d, J = 7.9 Hz, 2H), 7.57 – 7.39 (m, 5H), 7.20 (d, J = 8.3 Hz, 1H), 3.52 (s, 2H), 2.81 (t, J = 2.7 Hz, 1H), 2.35 (d, J = 17.3 Hz, 7H), 2.22 (s, 3H), 2.10 (t, J = 7.4 Hz, 2H), 2.00 (td, J = 7.4, 2.6 Hz, 2H), 1.54 (dt, J = 17.9, 7.4 Hz, 4H), 1.35 (s, 1H).

^{13}C NMR (101 MHz, $CDCl_3$) δ ppm: 165.38, 162.77, 160.61, 159.01, 151.45, 148.51, 137.82, 136.61, 134.97, 134.06, 132.71, 130.79, 129.39, 127.07, 125.51, 124.31, 123.74, 115.39, 113.25, 108.36, 82.80, 69.12, 62.40, 52.85, 52.52, 32.45, 31.92, 30.33, 29.69, 29.35, 27.22, 22.68, 17.66, 14.10, 13.30.

ESI-MS (m/z): 600.56 ([M+H+]).

Figure S2. The binding affinity of imatinib and imatinib probe to CD117 determined using SPR

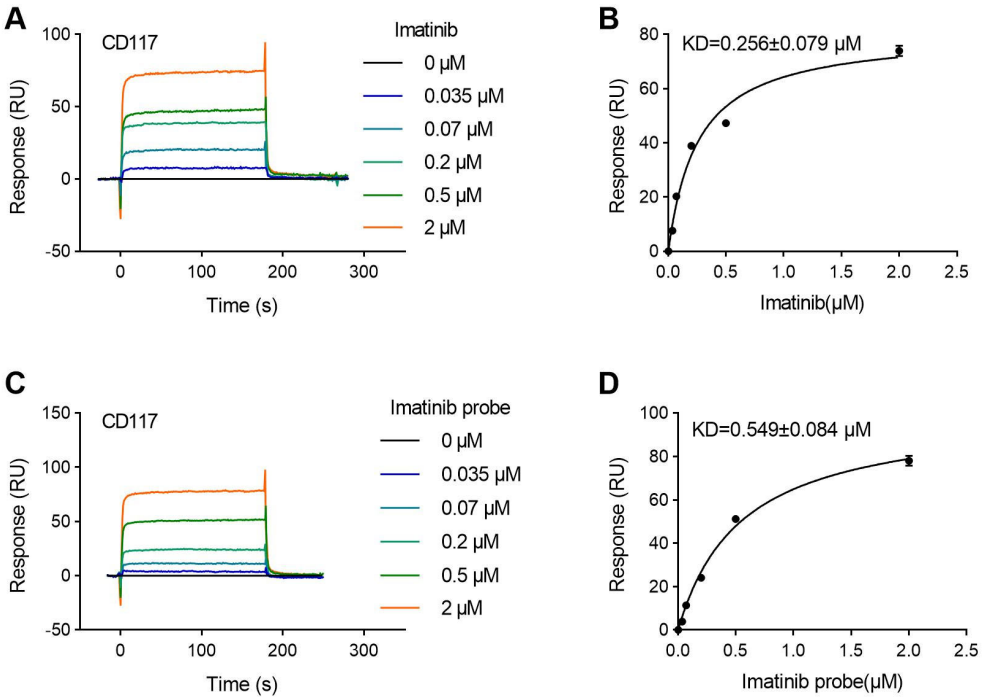

Table S1. Data used to evaluate the stability and reliability of N-Desmethyl imatinib probe staining

Fluorescence intensity	Sample	Background
Sample 1	23.780	0.850
Sample 2	23.570	1.060
Sample 3	20.620	0.880
Sample 4	24.160	0.880
Sample 5	23.670	0.990
Mean(μ)	21.360	0.962
Standard deviation(σ)	1.437	0.089

Figure S3. The ^{1}H NMR spectra of sorafenib probe

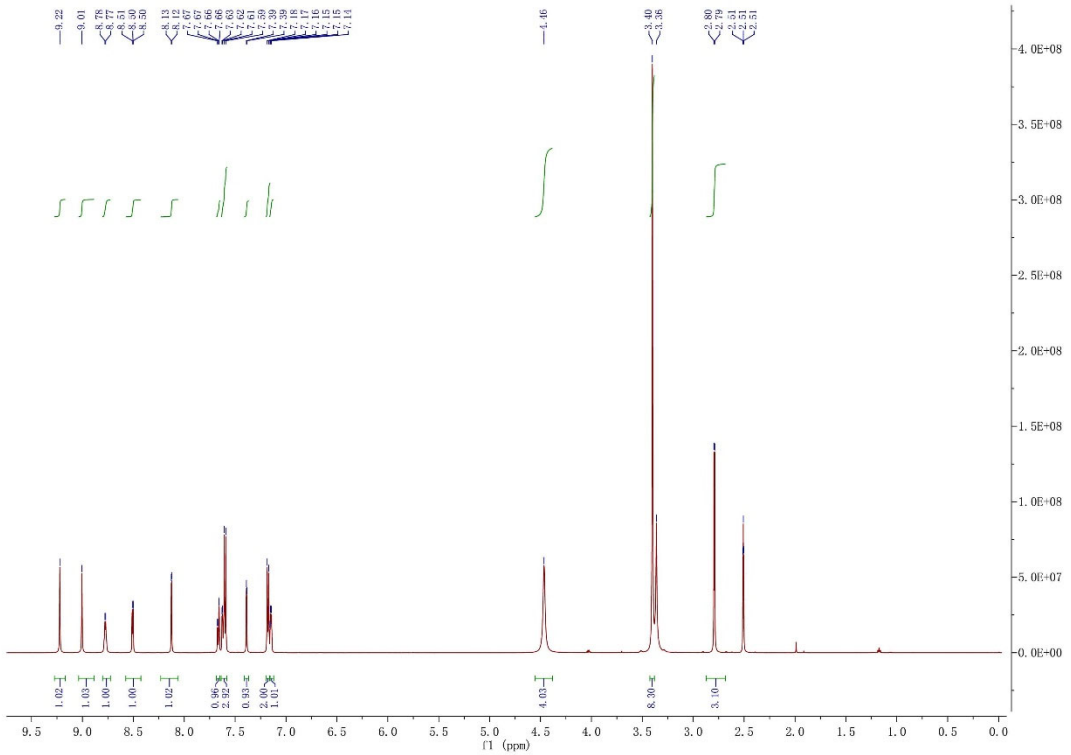

^{1}H NMR (400 MHz, $DMSO_{d6}$): δ 9.22 (s, 1H), 9.01 (s, 1H), 8.78 (d, J = 4.0 Hz, 1H), 8.50 (d, J = 4.0 Hz, 1H), 8.13 (s, 1H), 7.67 (m, 1H), 7.60 (m, J = 8.4 Hz, 2H), 7.39 (s, 1H), 7.18 (d, J = 8.4 Hz, 1H), 7.14(d, J = 4.0 Hz, 1H), 4.50 (br, 4H), 3.40 (s, 8H), 2.80 (s, 3H).

Figure S4. The binding affinity of sorafenib and sorafenib probe to VEGFR1 and VEGFR2 determined using SPR

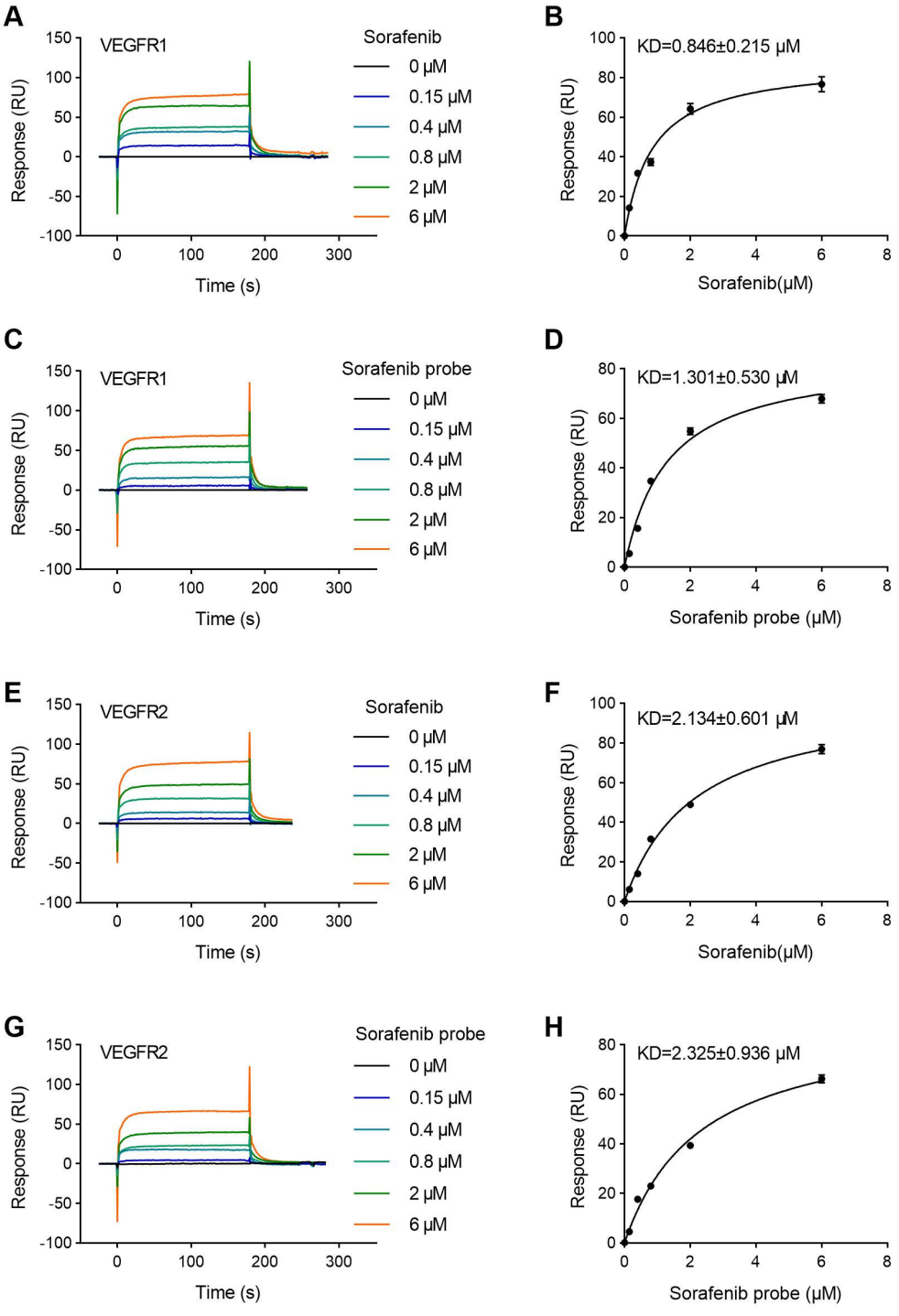

Table S2. Data used to evaluate the stability and reliability of sorafenib probe staining

Fluorescence intensity	Sample	Background
Sample 1	23.580	0.178
Sample 2	23.673	0.036
Sample 3	24.262	0.206
Sample 4	24.928	0.435
Sample 5	25.279	0.053
Sample 6	25.441	0.167
Sample 7	26.486	0.208
Sample 8	27.298	0.503
Sample 9	27.426	0.954
Sample 10	27.630	0.405
Mean(μ)	25.600	0.315
Standard deviation(σ)	1.459	0.260

Table S3. Patient information for sorafenib sensitivity testing

Patient ID	Staining intensity	Days to progression
1	32.602	42
2	55.029	153
3	68.186	93
4	50.994	132
5	55.581	231
6	82.664	426
7	80.545	168
8	51.921	176
9	45.71	53
10	53.129	118
11	32.99	54
12	51.813	71
13	72.895	328
14	26.942	23
15	53.834	127
16	25.387	5
17	49.54	66
18	29.999	16
19	52.68	84
20	29.536	45
21	34.671	75
22	29.051	36
23	71.307	197
24	79.204	254
25	78.397	393
27	74.081	287
28	65.336	204
29	81.675	84
30	78.622	302
31	73.592	225
32	84.837	485
33	79.442	243
34	62.832	189

Fig.S5 Meta-analysis showed that sorafenib had varying effects on different populations

(A) Meta-analysis literature was included in the process. (B) Therapeutic effect of sorafenib versus placebo on OS. (C) Therapeutic effect of sorafenib versus other targeted drugs on OS.

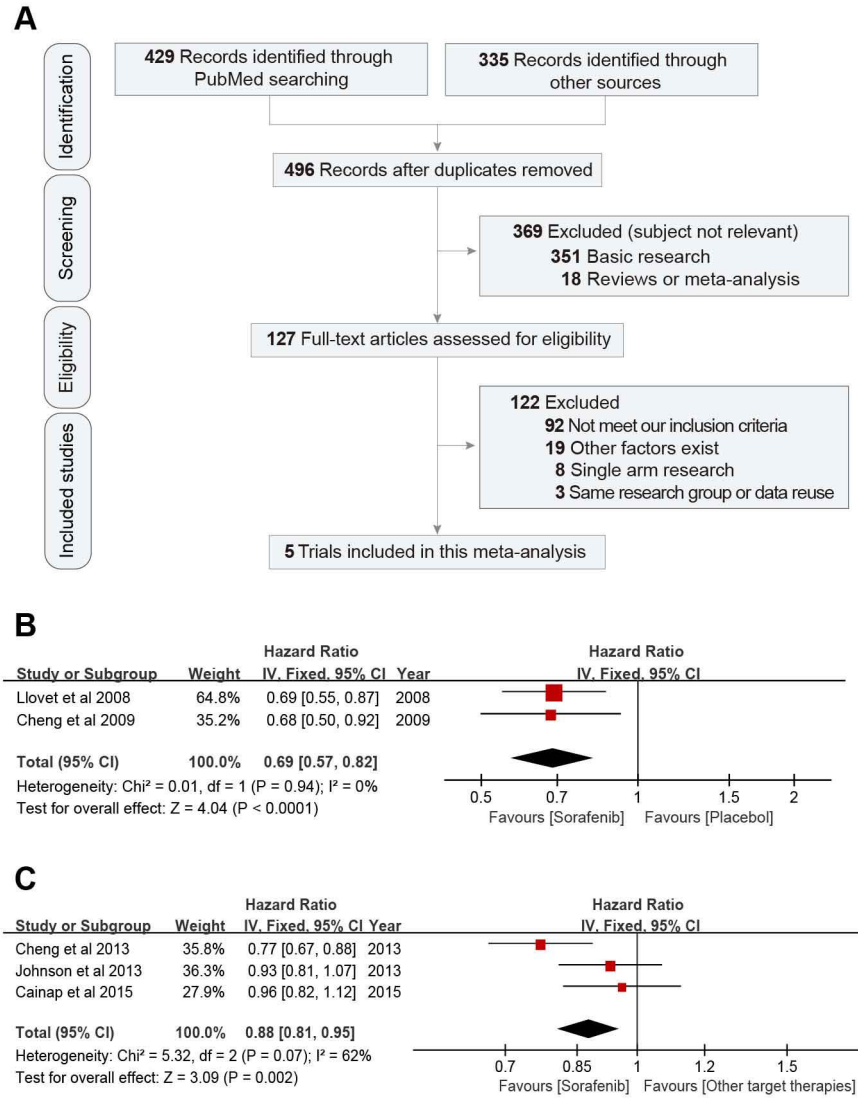

Table S4. Patient Demographics by trial

	Llovet et al.(Llovet et al., 2008)		Cheng et al.(Cheng et al., 2009)		Cheng et al.(Cheng et al., 2013)		Johnson et al.(Johnson et al., 2013)		Cainap et al.(Cainap et al., 2015)	
	2008		2009		2013		2013		2015	
	sorafenib	placebo	sorafenib	placebo	Sorafenib	sunitinib	sorafenib	brivanib	sorafenib	linifanib
Type	Superiority trial		Superiority trial		Superiority trial/non-inferiority trial		Non-inferiority trial		Superiority trial/non-inferiority trial	
N	299	303	150	76	544	530	578	577	521	514
Median age (years)	65[a]	66[a]	51	52	59	59	60	61	60	59
Male/Female	87/13	87/13	85/15	87/13	84/16	82/18	84/16	84/16	84/16	86/14
ECOG status (0/1/2)	54/38/8	54/39/7	25/69/5	28/67/5	53/47/0	53/47/0	61/39/0	64/36/0	66/34/0	63/37/0
BCLC grade(B/C)	18/82	17/83	5/95	4/96	16/84	13/87	17/78	17/77	20/80	16/84
Child–Pugh grade (A/B+C)	95/5	98/2	97/3	97/3	99/1	100/0	92/8	92/8	95/5	94/6
Cause of disease (HCV/HBV/ Alcohol)	29/11/26	27/9/26	11/71/nr	4/78/nr	22/53/15	21/55/17	21/45/14	20/44/18	25/53/12	25/54/13
Vascular invasion	36	41	36	34	38	43	27	27	41	46
Extrahepatic spread	53	50	69	68	38	36	50	49	57	60
Region (Asia/Other)	0/100	0/100	100/0	100/0	75/25	76/24	64/36	60/40	67/33	66/34
Quality score (Jadad score sheet)	5		5		4		4		5	

a, Data provided in the study are the average age. nr: not reported. ECOG PS, Eastern Cooperative Oncology Group performance status. BCLC, Barcelona Clinic Liver Cancer.

Table S5. Sorafenib versus placebo subgroup analysis on overall survival

Variable	sorafenib versus placebo
ECOG PS 0	**0.70 (0.53, 0.93); p < 0.01**
ECOG PS 1-2	**0.67 (0.53, 0.85); p < 0.01**
No extrahepatic spread	**0.52 (0.39, 0.71); p < 0.01**
Extrahepatic spread	0.84 (0.67, 1.05); p = 0.13
No macroscopic vascular invasion	**0.70 (0.55, 0.90); p < 0.01**
Macroscopic vascular invasion	**0.66 (0.51, 0.87); p < 0.01**
Neither macroscopic vascular invasion nor extrahepatic spread	**0.50 (0.33, 0.77); p < 0.01**
Macroscopic vascular invasion or extrahepatic spread	**0.76 (0.62, 0.93); p < 0.01**
Hepatitis B	0.74 (0.54, 1.03); p = 0.07

Results are expressed as HR and its 95% confidence interval.

Table S6. Sorafenib versus other target therapies (sunitinib/brivanib/linifanib) subgroup analysis on overall survival

Variable	**Sorafenib versus sunitinib/brivanib/linifanib**
Asian regions	**0.88 (0.78, 0.99); p = 0.03**
Non-Asian regions	0.81 (0.64, 1.02); p = 0.07
Patients with hepatitis B	0.98 (0.88, 1.10); p = 0.77
Patients with hepatitis C	**0.71 (0.56, 0.89); p < 0.01**
Non-HBV	0.87 (0.76, 1.00); p = 0.06
ECOG PS 0	0.94 (0.83, 1.07); p = 0.35
ECOG PS 1	0.93 (0.79, 1.10); p = 0.40
Macroscopic vascular invasion or extrahepatic spread	0.93 (0.82, 1.05); p = 0.24
Neither Macroscopic vascular invasion nor extrahepatic spread	1.00 (0.72, 1.39); p = 1.00

Results are expressed as HR and its 95% confidence interval.

Figure S6. Relationship between the expression of sorafenib known targets FLT1 and FLT3 and survival, stage or grade in HCC

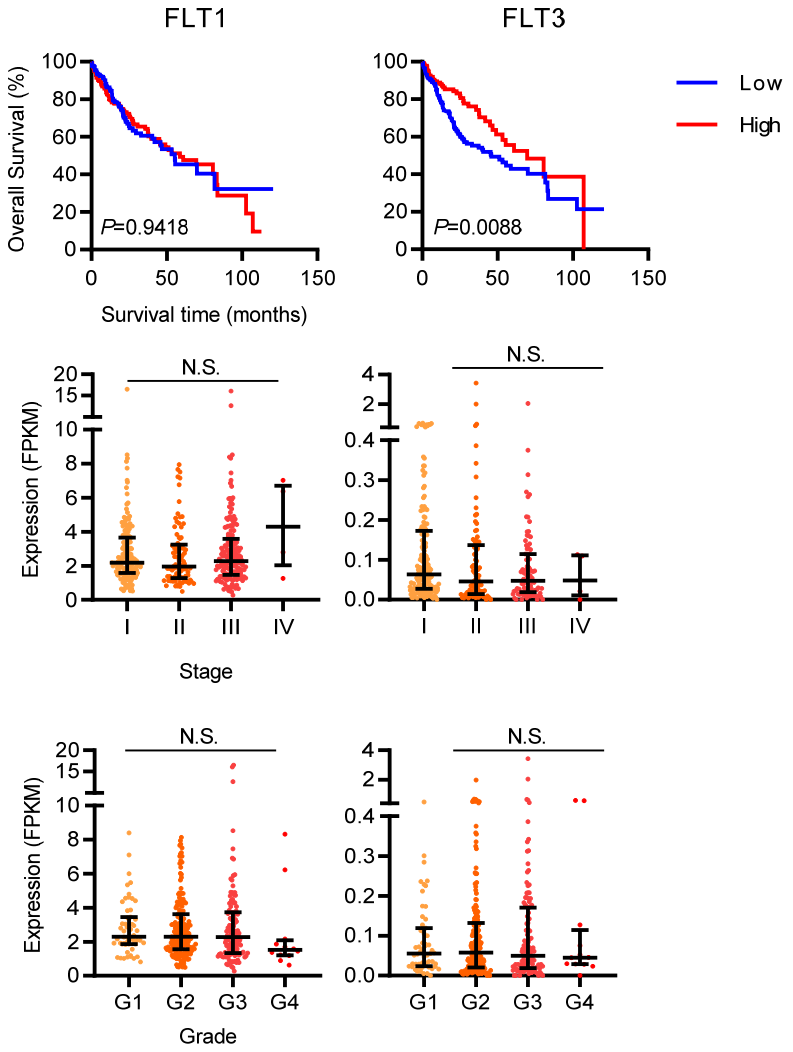

Table S7. Patient information of HCC tissue microarray

Patient ID	Age	Sex	Pathology diagnosis	Grade	Stage
1	39	M	Hepatocellular carcinoma	II-III	II
2	33	M	Hepatocellular carcinoma	II-III	II
3	47	M	Hepatocellular carcinoma	III	II
4	65	M	Hepatocellular carcinoma	III	II
5	52	M	Hepatocellular carcinoma	II	II
6	46	F	Hepatocellular carcinoma	III	IIIB
7	52	F	Hepatocellular carcinoma	III	I
8	47	M	Hepatocellular carcinoma	II	IIIA
9	41	M	Hepatocellular carcinoma	II	II
10	36	M	Hepatocellular carcinoma	II	II
11	61	M	Hepatocellular carcinoma	II	II
12	60	M	Hepatocellular carcinoma	II	II
13	52	M	Hepatocellular carcinoma	II	IIIA
14	44	M	Hepatocellular carcinoma	II	II
15	73	F	Hepatocellular carcinoma	II	IIIA
16	60	F	Hepatocellular carcinoma	I-II	II
17	18	M	Hepatocellular carcinoma	II	II
18	67	M	Hepatocellular carcinoma	II	II
19	43	M	Hepatocellular carcinoma	I	II
20	75	M	Hepatocellular carcinoma	I	IIIA
21	32	M	Hepatocellular carcinoma	II	II
22	50	F	Hepatocellular carcinoma	II	IIIB
23	57	M	Hepatocellular carcinoma	I-II	II
24	43	M	Hepatocellular carcinoma	I-II	IIIA
25	50	M	Hepatocellular carcinoma	I-II	IVA
26	42	M	Hepatocellular carcinoma	II	II
27	53	M	Hepatocellular carcinoma	II	II
28	40	M	Hepatocellular carcinoma	I-II	IIIA

29	55	M	Hepatocellular carcinoma	III	IIIA
30	42	F	Hepatocellular carcinoma	II	II
31	38	M	Hepatocellular carcinoma	II	II
32	40	M	Hepatocellular carcinoma	III	IIIA
33	55	M	Hepatocellular carcinoma	III	II
34	46	F	Hepatocellular carcinoma	II	II
35	47	M	Hepatocellular carcinoma	II	II
36	51	M	Hepatocellular carcinoma	II	IIIA
37	38	M	Hepatocellular carcinoma	III	IIIA
38	50	M	Hepatocellular carcinoma	II	II
39	43	M	Hepatocellular carcinoma	III	IIIA
40	58	M	Hepatocellular carcinoma	I-II	II
41	31	M	Hepatocellular carcinoma	I-II	II
42	44	M	Hepatocellular carcinoma	I	II
43	52	M	Hepatocellular carcinoma	II	II
44	48	M	Hepatocellular carcinoma	II	II
45	73	M	Hepatocellular carcinoma	III	II
46	50	F	Hepatocellular carcinoma	I	II
47	69	F	Hepatocellular carcinoma	II	II
48	66	M	Hepatocellular carcinoma	I-II	IIIA
49	53	M	Hepatocellular carcinoma	I	II
50	32	M	Hepatocellular carcinoma	II	II
51	62	M	Hepatocellular carcinoma	I	II
52	59	M	Hepatocellular carcinoma	II	II
53	79	F	Hepatocellular carcinoma	III	II
54	74	M	Hepatocellular carcinoma	II-III	IIIA
55	50	M	Hepatocellular carcinoma	II	II
56	67	M	Hepatocellular carcinoma	II	II
57	50	F	Hepatocellular carcinoma	I-II	IIIB
58	62	M	Hepatocellular carcinoma	I-II	IIIA

59	50	M	Hepatocellular carcinoma	III	IIIA
60	33	M	Hepatocellular carcinoma	II	IIIA
61	37	M	Hepatocellular carcinoma	I	IIIA
62	30	M	Hepatocellular carcinoma	II	IIIA
63	60	M	Hepatocellular carcinoma	III	IIIA
64	28	F	Hepatocellular carcinoma	II	IIIB
65	56	F	Hepatocellular carcinoma	I-II	IIIA
66	54	M	Hepatocellular carcinoma	III	IIIA
67	63	M	Hepatocellular carcinoma	II	IIIA
68	37	M	Hepatocellular carcinoma	III	II
69	61	M	Hepatocellular carcinoma	II	IIIA
70	35	M	Hepatocellular carcinoma	III	IIIA
71	17	F	Hepatocellular carcinoma	II	IIIA
72	35	M	Hepatocellular carcinoma	III	IIIA
73	48	M	Hepatocellular carcinoma	III	IIIA
74	72	M	Hepatocellular carcinoma	II	IIIA
75	58	M	Hepatocellular carcinoma	II	IIIA

Figure S7. Sorafenib probe staining intensity was not significantly different from gender and age

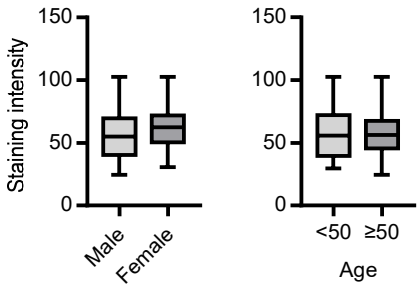

Figure S8. Representative images of sorafenib staining on HCC tissue microarray

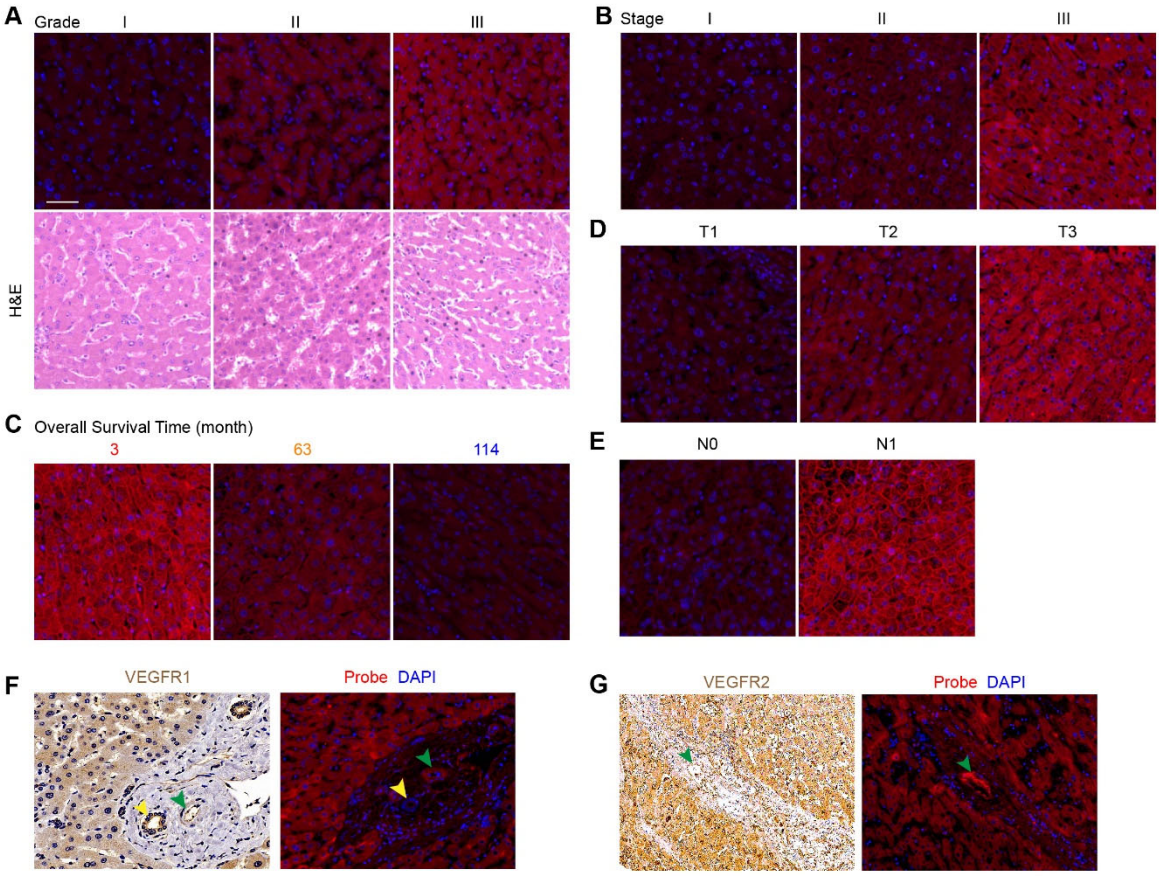

Figure S9. Different Sequence of probe staining and immunofluorescence staining

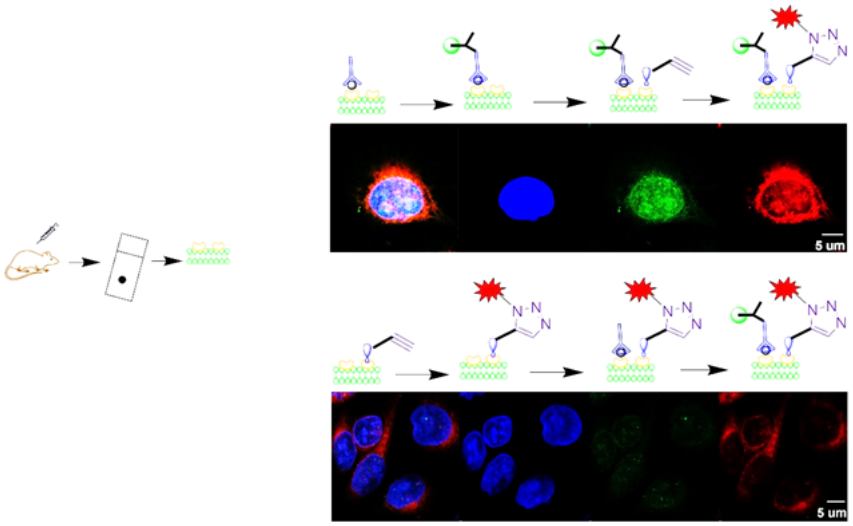

Transparent Methods

Materials

The following materials were used in this study: imatinib and sorafenib (MeilunBio, Dalian, China); CCK-8 kit (Beyotime Biotechnology, Shanghai, China); immunofluorescence staining kit with FITC-labeled goat anti-rabbit IgG and cell lines (KeyGEN BioTECH, Nanjing, China); antibodies to CD117, VEGFR2, PDGFR-β, p-VEGFR2, p-PDGFR-β (Affinity Bioreagents, Colorado, USA); Anti-Hepatocyte Specific Antigen antibody (Abcam).

Cell culture

GIST882, MHCC97H, MHCC97L, HepG2, Huh7 and PLC-PRF-5 cells were cultured in DMEM (HyClone), SNU-182, SNU-387, SNU-398, SNU-423, and SNU-449 cells were cultured in RPMI-1640 (HyClone) supplemented with 10% (v/v) fetal bovine serum (Thermo Fisher Scientific) at 37 °C in humidified atmosphere containing 5% CO_2. The cell lines were tested to determine the presence of *Mycoplasma* before use. Cell identification was provided by KeyGen Biotech (Nanjing, China).

Cell proliferation assay

CCK-8 assay determines the cell proliferation. PLC-PRF-5, MHCC-97L, and MHCC-97H (5×10^3 cells/mL) were seeded in 96-well culture plates ($n = 3$). After overnight incubation, the cells were treated with various concentrations of N-desmethyl imatinib, N-desmethyl imatinib probe, sorafenib, or sorafenib probe. After 48 h incubation, cell viability was measured after the addition of 10 μL CCK-8 solution at 37 °C for 2 h. Optical density was determined at 450 nm with a microplate reader (Multiskan™ FC, Thermo Scientific, Waltham, MA, USA). The ratio of absorbance to the control group was analyzed by nonlinear regression analysis using GraphPad Prism version 7 for Windows to obtain the IC_{50} value.

Synthesis of sorafenib probe

Under dark conditions, $[Pd(cinnamyl)Cl]_2$ (1.6 mg, 0.5 mol%), RockPhos (8.4 mg, 1.5 mol%), Cs_2CO_3 (391 mg, 1.2 mmol), and toluene (5 mL) were added to a glass vial that was sealed with a screw cap fitted with a PTFE/silicone septum and removed from the glovebox. Sorafenib (279 mg, 0.60 mmol) and alcohol (100 mg, 0.72 mmol) in 1 mL of toluene were then added using a microsyringe. The vial was then placed on a temperature-controlled aluminum plate set to 90 °C, and the solution was stirred for 16 h. Afterward, the vial was removed from the heating block and cooled to room temperature. An aliquot was filtered through a small plug of silica that was then washed with dichloromethane, and the solvent was evaporated under reduced pressure. The crude product was subjected to macroporous resin column chromatography (methanol/water) to produce the probe (125.8 mg, 37%).

Patient samples and ethics

We complied with all relevant ethical regulations. We collected more than 300 paraffin-embedded specimens of patients with HCC and analyzed the clinical data integrity. A total of 33 patients took sorafenib after they underwent surgery. Their paraffin specimens were used for sorafenib probe staining detection. The staining results were further conducted correlation analysis with clinical data. These

cases were from Tianjin Medical University General Hospital, Tianjin Cancer Hospital, Beijing Shunyi Hospital, Shandong Shouguang Hospital, Tangshan Coal Hospital, Shanxi Houma People's Hospital, 541st Hospital of the Chinese People's Liberation Army, Liaoning Provincial People's Hospital and Huashan Hospital Affiliated to Fudan University.

Probe staining assay for cells

A 24-well plate with a climbing film was plated with about 7×10^4 log phase cells, and 500 μL of the complete medium was added to each well. After 9 h, the probe was added (final concentration: 10 μM), and an equal amount of DMSO was added to the control group. After incubation for 8 h, the medium was discarded, PBS was immersed thrice for 3 min, and 200 μL of cold methanol was added for 20 min at room temperature. Thereafter, methanol was discarded, and PBS was immersed thrice for 3 min and irradiated with ultraviolet light (365 nm) for 1 h. The cells were incubated with 0.1% TritonX-100 for 10 min, washed with PBS thrice for 3 min, added with 5% FBS in PBS solution, and blocked at room temperature for 30 min. The cells were washed thrice with PBS and added with a clicking reaction solution for 1 h, but the solution was protected from light exposure. The cells were washed four times with PBS until they became colorless. Finally, the cells were stained with DAPI and photographed using a laser confocal microscope (Leica, Germany) under the same acquisition condition. Images of the probe fluorescent staining channels were analyzed with ImageJ and the mean fluorescence intensity of each sample was calculated.

Probe staining assay for sections

Paraffin sections were immersed in xylene for 15 min, dewaxed with xylene II for 15 min, placed in 100% alcohol for 5 min, 100% alcohol II for 5 min, 95% alcohol for 5 min, 80% alcohol for 5 min, tap water for 5 min, rinsed with distilled water for 3 min, and washed with PBS thrice for 3 min for rehydration. The tissue sections were then placed in a 50-fold diluted EDTA (pH 8) repair solution, preheated in a microwave defrost mode for 6 min until it slightly boiled, and maintained at low and medium heat for 15 min. Afterward, the cells were naturally cooled for 20–30 min for antigen retrieval and then immersed in PBS thrice for 3 min. The PBS outside the specimen was wiped off with a filter paper and placed in a humid chamber. Subsequently, 0.3% Triton X-100 was added dropwise and incubated for 10 min at room temperature. The cells were immersed in PBS thrice for 3 min at each time, after which 2% BSA was added for 30 min. The tissue was incubated with probe solution (10 μM) for 1 h at 37 °C, and the control group was added with the same amount of PBS. The tissue was immersed in PBS thrice for 3 min. PBS was added to cover the tissue, which was exposed to UV light (365 nm) for 1 h. Thereafter, the working solution of the click solution was added for the click reaction for 2 h and immersed in PBS four times for 3 min at each time, washed until the samples became colorless, and sealed with DAPI. The samples were photographed with a laser confocal microscope or a slice scanner under the same acquisition condition. Images of the probe fluorescent staining channels were analyzed with ImageJ and the mean fluorescence intensity of each sample was calculated.

Catching targets using the probe

The log phase cells were incubated with the probe (final concentration 10 μM) for 8 h, and the medium was discarded. A total of 400 μL of RIPA strong lysate was added to each dish and allowed to stand for

30 min on ice. The cells were scraped and transferred to an EP tube. The samples were centrifuged at 12,000 rpm for 10 min at 4 °C. The supernatant was obtained, and the click reaction solution was added for 1 h. The small molecule was treated with a 5 kD ultrafiltration tube and 30 μL of streptavidin magnetic beads. The mixture was incubated overnight at 4 °C with gentle rotation. The cells were washed four times with RIPA weak lysate, stained with Coomassie blue via SDS-PAGE, and identified through mass spectrometry after in-gel digestion was conducted.

Molecular docking

KIT (ID 1PKG), BRAF (ID 4E26), RAF1 (ID 3OMV), VEGFR1 (ID 3HNG), and VEGFR2 (ID 2XIR) in PDB file format were downloaded from the Protein Data Bank(Berman, 2000). Imatinib and sorafenib in SDF file format were downloaded from PubChem(Kim et al., 2016). Molecular docking was performed using Schrödinger Maestro 8.0. The ligand and protein complex were saved in PDB file format and further analyzed with Pymol 2.2.

Surface plasmon resonance (SPR) assay

SPR experiments were performed using a Biacore 3000 instrument (GE Healthcare, Piscataway, NJ, USA) at 25°C. CD117 was purchased from Novus Biologicals, and VEGFR1 and VEGFR2 were purchased from Sigma-Aldrich. CD117, VEGFR1, and VEGFR2 were immobilized on CM5 sensor chips using the Biacore Amine Coupling Kit in accordance with the manufacturer's instructions. Briefly, the chip was activated using a 1:1 mixture of 0.2 M N-ethyl-N'-(3-dimethylaminopropyl) carbodiimide and 0.05 M N-hydroxysuccimide at 10 μL/min for 7 min. CD117, VEGFR1, and VEGFR2 were coated on the chip at 150 μg/mL in 10 mM sodium acetate buffer (pH 5.0) for 2.5, 3.5, 3 min at 10 μL/min to a level of 8700, 9200, 9800 response units. The unoccupied binding sites were blocked using 1 M ethanolamine at pH 8.5. N-desmethyl imatinib, N-desmethyl imatinib probe, sorafenib and sorafenib probes were dissolved to 10 mM by 100% DMSO and diluted to 10 μM by 1×PBS (pH 7.4). Finally, a series of analytes (N-desmethyl imatinib and N-desmethyl imatinib ranging from 0.035–2.0 μM, sorafenib and sorafenib probe ranging from 0.15-6.0 μM) was used as kinetic analytes. (Theoretical Rmax: Imatinib-CD117 38.36 RU, Imatinib probe-CD117 30.67 RU, sorafenib-VEGFR1 84.51 RU, sorafenib probe-VEGFR1 103.01 RU, sorafenib-VEGFR2 36.86 RU, sorafenib probe-VEGFR2 44.93 RU.) 1×PBS (pH 7.4, 0.1% DMSO) was used as the running buffer for analyte dilution. All buffers were filtered and degassed prior to use. For kinetic analysis, a blank cell without protein was used as the reference cell and performed other operations as mentioned before, and the data were analyzed using the BIA evaluation software (Version 4.1).

Immunofluorescence staining

The cells were fixed with 4% formaldehyde in phosphate-buffered saline (PBS) for 5 min, permeabilized with 0.2% Triton X-100, blocked with 3% bovine serum albumin, and incubated overnight with primary antibodies at 4 °C. FITC-labeled secondary antibodies were incubated for 1 h at room temperature. Each step was followed by two washing procedures with for 5 min. Finally, the cells stained with 4′,6-diamidino-2-phenylindole (DAPI; Sigma, USA) were mounted and viewed using a laser scanning confocal microscope A1 (Nikon, Japan). The sequence of probe staining and immunofluorescence staining was tested. (Fig. S7)

Preparation of tissue microarrays

GIST tissue microarrays containing 24 cases and HCC tissue microarrays consisting of 75 cases were purchased from the US Biomax for IHC and probe staining. Tissue blocks of the tissue array were collected within 5 years. Each single tissue spot on every array slide was individually examined by certified pathologists in accordance with the published standardizations of the World Health Organization for diagnosis, classification, and pathological grade. The hospital and the patients consented to include the specimens in the study. All tissues were collected under the highest ethical standards. Each donor was completely informed and provided consent. All human tissues were collected under Health Insurance Portability and Accountability Act (HIPPA)-approved protocols. Probe staining and immunohistochemical staining were performed on the tissue microarrays with the same sample distribution, and results of the same sample were continuously observed.

Uniformity and signal variability assessment of the probe staining assay

To evaluate the stability and reliability of the probe staining system, we analyzed the staining performance of the probe on the basis of the signal-to-background ratio (S/B), signal-to-noise ratio (S/N), coefficient of variation (CV) and Z-factor (Z') by using the following formula: (Zhang et al., 1999)

$$S/B=\frac{\mu_s}{\mu_b}$$

$$S/N=\frac{\mu_s-\mu_b}{\sigma_b}$$

$$CV=\frac{\sigma}{\mu}\times 100\%$$

$$Z'=1-\frac{3\times(\sigma_s+\sigma_b)}{\mu_s-\mu_b}$$

where μ, σ, s, and b represent the mean, standard deviations, signal, and background, respectively.

Super-resolution (STORM) imaging

The colocalization of the imatinib probe with CD117 was observed with Nikon Super-Resolution Microscope N-STORM. Immediately before imaging was conducted, the samples were covered with an imaging medium freshly prepared in accordance with the manufacturer's instructions (Dudok et al., 2015), containing 5% (m/v) glucose, 0.1 M mercaptoethylamine, 1 mg mL^{-1} glucose oxidase and catalase (2.5 μL mL^{-1} of aqueous solution from Sigma, approximately 1,500 U mL^{-1} final concentration) in Dulbecco's PBS (Sigma). Finally, coverslips were sealed with nail polish, and the slides were transferred to the microscope setup after 10 min. STORM imaging was performed for up to 3 h after the specimens were covered. STORM images were processed using the N-STORM module in NIS-Elements AR.

Western blot analysis

Cells were washed with PBS and lysed in ice-cold lysis buffer with protease Inhibitor Cocktail (Sigma) on ice for 30 min. Lysates were separated through electrophoresis and transferred onto polyvinylidene difluoride membranes (Millipore). The membranes were blocked, incubated with primary antibody against CD117 (1:1,000, Affinity), VEGFR2 (1:1,000, Affinity), PDGFR-β (1:1,000, Affinity), p-VEGFR2 (1:1,000, Affinity), and p-PDGFR-β (1:1,000, Affinity) at 4 °C overnight, and incubated with a horseradish

peroxidase-conjugated goat anti-rabbit IgG secondary antibody (Thermo Scientific) for 1 h at room temperature. Protein expression was assessed using an enhanced chemiluminescent substrate (Millipore) and exposed to a chemiluminescent film.

Cell-derived xenograft model

Animal experiments were conducted in accordance with the National Institutes of Health Animal Use Guidelines. All of the experimental protocols were approved by the Institutional Animal Care and Use Committee at Tianjin International Joint Academy of Biomedicine. A total of 1×10^7 cells were injected subcutaneously to nude mice. When tumor volume reached approximately 50 mm^3, the mice were treated with 30 mg/kg sorafenib or the vehicle. The diameters of the tumors were serially measured with a digital caliper every 3 days, and their volumes were calculated using the following formula: volume = (length × $width^2$)/2. The mice were euthanized 25 days after cell injection. The tumors were sectioned into paraffin sections and then stained and analyzed by probe staining assay for sections. The tumor inhibition rate was calculated by the following formula: tumor inhibition rate = 1 − mean tumor volume (sorafenib) / mean tumor volume (control).

Bioinformatics analysis

The clinical information and gene expression data of liver hepatocellular carcinoma in The Cancer Genome Atlas (TCGA) were downloaded using the R package TCGAbiolinks(Colaprico et al., 2016) and analyzed via GraphPad Prism version 7.00. Principal component analysis (PCA) was performed using SIMCA 14.1. COX regression analysis was conducted with SPSS 21.0. Gene set enrichment analysis (GSEA) was carried out using R package clusterProfiler(Yu et al., 2012).

Statistical analysis

Statistical analyses were performed using GraphPad Prism version 8 for Windows and R 3.5.1. Statistically significant differences were calculated using Student's *t*-test, one-way ANOVA, Pearson's correlation, and Kaplan–Meier as needed. $P < 0.05$ was considered significant.

References

Berman, H.M. (2000). The Protein Data Bank. Nucleic Acids Research *28*, 235-242.
Cainap, C., Qin, S., Huang, W.T., Chung, I.J., Pan, H., Cheng, Y., Kudo, M., Kang, Y.K., Chen, P.J., Toh, H.C.*, et al.* (2015). Linifanib versus Sorafenib in patients with advanced hepatocellular carcinoma: results of a randomized phase III trial. J Clin Oncol *33*, 172-179.
Cheng, A.L., Kang, Y.K., Chen, Z., Tsao, C.J., Qin, S., Kim, J.S., Luo, R., Feng, J., Ye, S., Yang, T.S.*, et al.* (2009). Efficacy and safety of sorafenib in patients in the Asia-Pacific region with advanced hepatocellular carcinoma: a phase III randomised, double-blind, placebo-controlled trial. Lancet Oncol *10*, 25-34.
Cheng, A.L., Kang, Y.K., Lin, D.Y., Park, J.W., Kudo, M., Qin, S., Chung, H.C., Song, X., Xu, J., Poggi, G.*, et al.* (2013). Sunitinib versus sorafenib in advanced hepatocellular cancer: results of a randomized phase III trial. J Clin Oncol *31*, 4067-4075.
Colaprico, A., Silva, T.C., Olsen, C., Garofano, L., Cava, C., Garolini, D., Sabedot, T.S., Malta, T.M., Pagnotta, S.M., Castiglioni, I.*, et al.* (2016). TCGAbiolinks: an R/Bioconductor package for integrative analysis of TCGA data. Nucleic Acids Res *44*, e71.
Dudok, B., Barna, L., Ledri, M., Szabo, S.I., Szabadits, E., Pinter, B., Woodhams, S.G., Henstridge, C.M., Balla, G.Y., Nyilas, R.*, et al.* (2015). Cell-specific STORM super-resolution imaging reveals nanoscale organization of cannabinoid signaling. Nat Neurosci *18*, 75-86.
Johnson, P.J., Qin, S., Park, J.W., Poon, R.T., Raoul, J.L., Philip, P.A., Hsu, C.H., Hu, T.H., Heo, J., Xu, J.*, et al.* (2013). Brivanib versus sorafenib as first-line therapy in patients with unresectable, advanced hepatocellular carcinoma: results from the randomized phase III BRISK-FL study. J Clin Oncol *31*, 3517-3524.
Kim, S., Thiessen, P.A., Bolton, E.E., Chen, J., Fu, G., Gindulyte, A., Han, L., He, J., He, S., Shoemaker, B.A.*, et al.* (2016). PubChem Substance and Compound databases. Nucleic Acids Res *44*, D1202-1213.
Llovet, J.M., Ricci, S., Mazzaferro, V., Hilgard, P., Gane, E., Blanc, J.F., de Oliveira, A.C., Santoro, A., Raoul, J.L., Forner, A.*, et al.* (2008). Sorafenib in advanced hepatocellular carcinoma. N Engl J Med *359*, 378-390.
Yu, G., Wang, L.G., Han, Y., and He, Q.Y. (2012). clusterProfiler: an R package for comparing biological themes among gene clusters. OMICS *16*, 284-287.
Zhang, J.H., Chung, T.D., and Oldenburg, K.R. (1999). A Simple Statistical Parameter for Use in Evaluation and Validation of High Throughput Screening Assays. J Biomol Screen *4*, 67-73.